A DFT STUDY ON THE COMPLEXATION OF METAL CATIONS BY THE PROTEIN α-SYNUCLEIN

Rafael Ramis Cortés

Master's Thesis

Master's degree in Theoretical Chemistry and Computational Modeling

at the

UNIVERSITAT DE LES ILLES BALEARS

Academic year 2015/2016

September 2016

Author's signature

Supervisor:
Dr. Juan Frau Munar

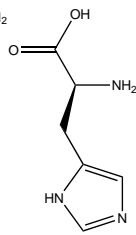Co-Supervisor:
Dr. Joaquín Ortega Castro

Contents

Amino acids

Arginine
Arg, R

Histidine
Hid, H
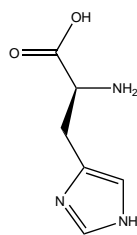
Histidine
Hie, H
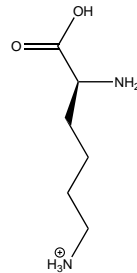
Lysine
Lys, K
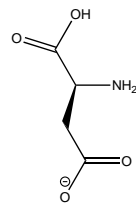
Aspartate
Asp, D
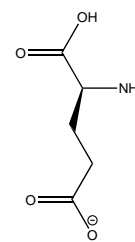
Glutamate
Glu, E
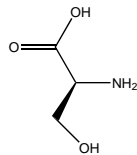
Serine
Ser, S
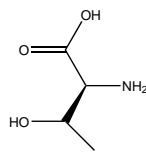
Threonine
Thr, T
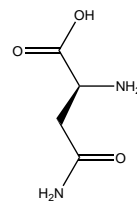
Asparagine
Asn, N
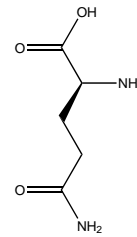
Glutamine
Gln, Q
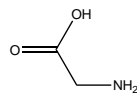
Glycine
Gly, G
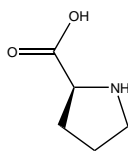
Proline
Pro, P
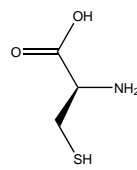
Cysteine
Cys, C

Selenocysteine
Sec, U

Alanine
Ala, A

Valine
Val, V

Isoleucine
Ile, I

Leucine
Leu, L

Phenylalanine
Phe, F

Tyrosine
Tyr, Y

Tryptophan
Trp, W

Methionine
Met, M

N-acetylmethionine
NacMet
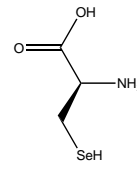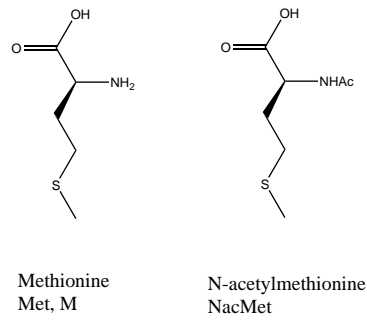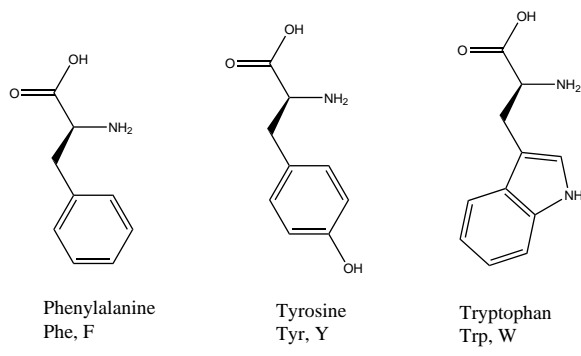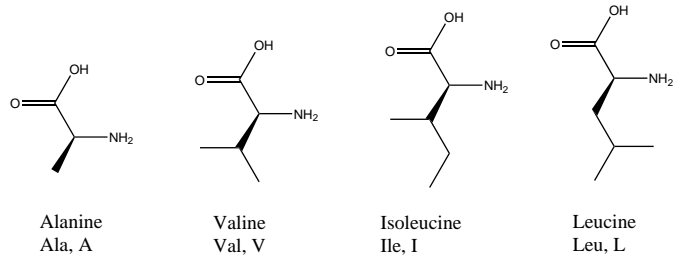
Chapter 1

Introduction

1.1 Parkinson's disease

1.1.1 Symptoms and pathogenesis

Parkinson's disease (PD) is the second most common neurological disorder after Alzheimer's [1]. Between 1 and 2 % of the population above 65 years and about 4 % of those above 85 are affected by it [2]. It occurs in roughly the same proportion of men and women, with a slight preponderance of affected men. Although the average age of onset is 59 years, it may appear at any age, even under 20 [3].

PD was first described by Dr. James Parkinson [4] in 1819. Its most noticeable symptoms include tremor, stiffness of muscles, bradykinesia (slow movements) and loss of balance and coordination. Although it is a general belief, not every PD patient experiences tremor; only about 70 % of them do. Other manifestations, which are usually less evident but which are also reported by patients, are sleeping difficulties, swallowing problems, anxiety, depression, mood disorders, hallucinations, memory loss, speech problems, incontinence, constipation, falls or dizziness [5].

To understand the motor symptoms, it is convenient to know about the processes that lead to the execution of voluntary movements and the effects of PD on them.

The brain is made up of three main parts: the cerebral hemispheres (known as the *cerebrum*), the *cerebelum* and the *brain stem*. At the base of the brain there are the *basal ganglia*, which contain the *striatum* (made up of the *caudate* and the *putamen*) and the *globus pallidus*. Under the basal ganglia, there is a very small region called the *substantia nigra*, divided into the *substantia nigra pars compacta* and the *substantia nigra pars reticulata*. The name "substantia nigra" means "dark substance" and it is due to the fact that neuromelanin accumulates inside the neurons in this region. Figure 1.1 depicts the location of these structures.
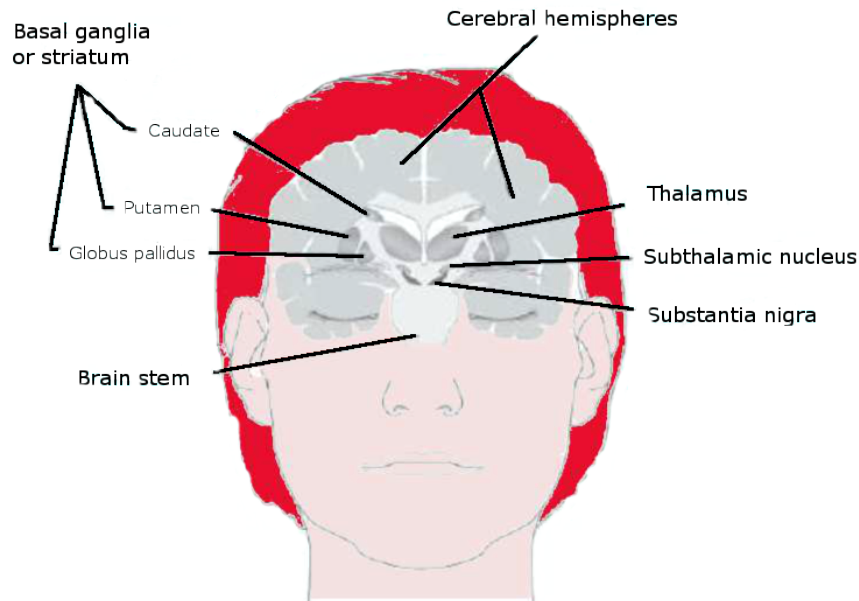
Figure 1.1: Relative location of the structures that are important in normal motor control. Modified from Ref. [6].

When someone decides to make a movement, a signal is generated on the surface of the cerebrum (the *cerebral cortex*) and travels along the neurons' axons towards the basal ganglia, which modify it and send it to another

cerebral structure, the *thalamus*, from which it returns to the cortex, and the process is repeated until the signal is properly modulated. At this moment, it is sent to the muscles and this causes them to contract and the movement to take place.

All these signal transmissions are enabled by the so called *neurotransmitters*. These are chemicals whose production is stimulated by the signals at the end of the axons and which travel to the next neuron through the *synapses* (the small spaces between the neurons) and are recognized by specific receptors. There are a wide variety of neurotransmitters, including dopamine, acetylcholine, norepinephrine, serotonin or glutamate, which work in coordination. The substantia nigra pars compacta is full of dopamine-producing neurons, whose product is sent to the striatum (accordingly, this path is termed the *nigrostriatal path*). Symptoms of PD appear when about 50 % of these neurons are damaged, since the lack of dopamine disrupts the workings of the whole system [6]. A distinctive feature of this disease is the presence of the so called *Lewy bodies*, described as eosinophilic, round, intracytoplasmic inclusions with a core, a body and a halo (see figure 1.2) in the surviving cells of the substantia nigra. These structures also appear in other neurodegenerative diseases such as dementia with Lewy bodies (DLB), although with a more widespread distribution in the brain [7].
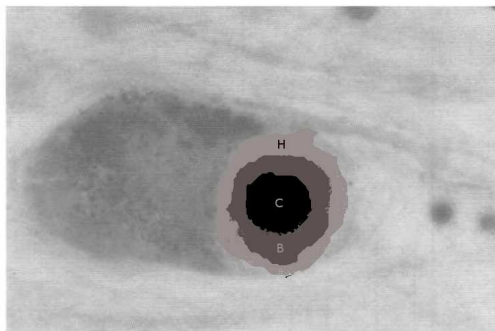
Figure 1.2: Lewy body with core (C), body (B) and halo (H). x 2625. Modified from Ref. [7].

1.1.2 Treatment

Up to date, no cure is known for PD. The main symptoms, such as tremors and rigidity of muscles, can be eased by the practice of physical exercise on a day-to-day basis, as demonstrated e.g. by the fact that, since 2012, several clinical trials have shown that using the Nintendo Wii regularly may have a positive impact on PD patients' quality of life [8, 9, 10] and that it constitutes an objective way of assessing the severity of the disease in each particular case [11, 12]. Apart from this, the symptoms are treated mainly by means of drugs. The most popular and effective ones are (L)-3,4-dihydroxyphenylalanine (commonly known as levodopa) and several dopamine agonists. These drugs and some additional ones are presented in Table 1.1.

Besides medications, surgery is also used sometimes to tackle some of the PD symptoms. Appropriate candidates for it are those patients in an advanced stage of the disease for whom drugs are no longer effective against motor symptoms (tremor, bradykinesia, dyskinesia) but they are for non-motor ones, and that do not suffer from major unstable psychiatric conditions (depression, psychosis). There are two main types of PD surgery: ablative (or lesion) surgery and Deep Brain Stimulation (DBS) [20]. The former implies causing a small, precise lesion at some region of the brain, usually the *globus pallidus* (pallidotomy) or the thalamus (thalamotomy). Pallidotomy has been found to be effective in supressing the tremor and increasing the agility of hands and arms [21, 22]. Similar effects have been demonstrated for thalamotomy [23, 24]. Nowadays, however, DBS is preferred over ablative surgery due to its reversibility, adjustability and higher safety [3], while having the same benefits attributed to ablation [25]. The main target for DBS is the subthalamic nucleus (STN), and it is even able to improve non-motor symptoms [26]. An excellent review of the history of the DBS technique is given in Ref. [27].

Table 1.1: Main families of drugs used against Parkinson's disease, with the main representatives of each one and their known side effects. L. T. = Levodopa therapy; D. A. = Dopamine agonists; M-B I. = MAO-B inhibitors; A. = Anticholinergics.

Family	Examples	Side effects	Comments
L. T.	Levodopa, carbidopa, benserazide, entacapone, tolcapone	Nausea, wearing-off, confusion, hallucinations, orthostatic hypotension (levodopa) [13], urine decoloration (entacapone), hepatotoxicity (tolcapone) [14]	Levodopa is a dopamine precursor undergoing a decarboxylation. Carbidopa and benserazide are used with levodopa. Entacapone and tolcapone are cathecol-O-methyltransferase (COMT) inhibitors [14]
D. A.	Bromocriptine, pramipexole, ropinirole, apomorphine, pergolide, lisuride, rotigotine [13, 15]	Insomnia, headache, confusion, constipation, vomiting, hypotension, nausea, dizziness, dyskinesia, hallucinations, erythema and pruritus (rotigotine), sleep attacks, psychosis, hypersexuality, penile erection, yawning, sedation, subcutaneous nodules, haemolytic anemia, heart failure (pergolide) [14, 16, 17]	They mimic dopamine, making the brain act as if there were enough, and can be used in combination with levodopa or on their own, but are not as effective as it [14]
M-B I.	Selegiline, rasagiline, safinamide	Hypertension, "serotonine syndrome", with fever, hallucinations, tachycardia or gastrointestinal symptoms [18]	"MAO" stands for "monoamine oxidase", an enzyme that oxidatively deaminates monoamines, including dopamine, and comes in two isoforms (A and B). Safinamide is on an experimental phase. They are less efective than dopamine agonists, but with fewer side effects [18]
A.	Trihexyphenidyl, benztropine, biperiden, amantadine [3, 19]	Dry mouth, decreased memory, confusion, blurred vision, difficulty with urination, constipation [3]	They block interactions between acetylcholine and dopamine receptors, relieving tremor. Amantadine is also an NMDA (N-methyl-D-aspartate) antagonist. NMDA is a glutamate receptor, and glutamate levels increase in PD due to an excessive activity of the subthalamic nucleus (STN), generating dyskinesias [19]

1.1.3 Etiology

The etiology of PD (that is, the set of factors that lie at the origin of the disease) is not fully understood yet. Most experts believe that it is caused by a combination of both environmental and genetic factors, but they disagree on their relative importance.

1.1.3.1 Evidence for an enviromental origin

One of the most striking early pieces of evidence supporting the environmental hypothesis was reported in 1983 by Dr. J. William Langston [28]. Four people developed Parkinson-like symptoms after using a designer drug, later identified as 1-methyl-4-phenyl-1,2,3,6-tetrahydropyridine (MPTP) with trace amounts of 1-methyl-4-phenyl-4-propionoxy-piperidine (MPPP). Their responses to typical PD medications such as levodopa resembled the ones of PD patients, and an autopsy later determined that their dopaminergic neurons in the substantia nigra had been damaged.

Just after this episode, researchers wanted to gain some insights into the molecular mechanisms underlying the neurotoxicity of MPTP, assuming that this knowledge would provide a better understanding of PD pathogenesis. As a result, a series of papers addressing this question were published in the following years [29, 30, 31]. In all of them, a metabolite of MPTP known as 1-methyl-1,4-phenylpyridinium (MPP+) was identified as the active toxic compound. This molecule has a high affinity for dopamine transporters located at the membrane of the dopaminergic neurons that allows it to enter them. Once inside, they may access the mitochondria and interfere with the cellular respiration process by blocking the so called *complex I*, leading to an insufficient production of ATP, an increased generation of free radicals and, eventually, neuronal death [32].

The discovery of this correlation between MPTP/MPP+ intake and the development of Parkinson-like symptoms reinforced the idea that PD is

18

mainly caused by environmental agents, since the chemical structure of MPP+ is strikingly similar to that of paraquat (1,1'-dimethyl-4,4'-bipyridinium ion), a widely used herbicide (see figure 1.3 for a comparison). This and other pesticides have been shown to affect the dopaminergic systems in animals. See Ref. [33] for a comprehensive review of the literature on environment and PD.

(a)   **(b)**
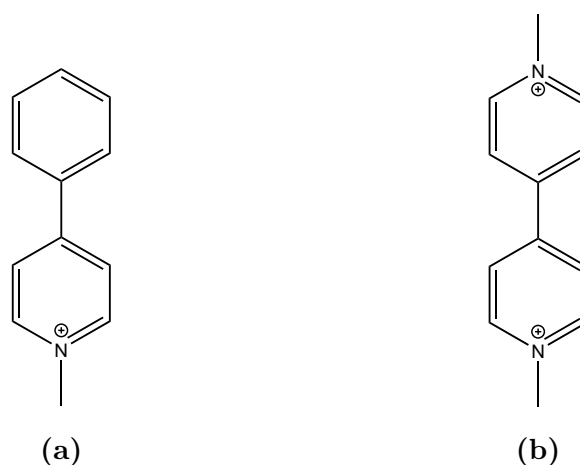
Figure 1.3: (a): MPP+. (b): Paraquat. Note the similarity between both structures.

1.1.3.2   Evidence for a genetic origin

The fact that PD only affects about 2 % of the population in a specific age range persuaded most experts of the existence of a genetic factor involved in the etiology of the disease [3] that increases susceptibility to the toxicity of the exogenous agents that cause it, whichever they are. This encouraged the conduction of several genetic studies at the same time as the environmental ones. Many case-control studies concluded that relatives of patients had a higher probability of being affected themselves than relatives of controls [34, 35, 36] and that a positive familial history of PD was stronger as a risk factor than exposure to the environmental agents mentioned above [37]. On the other hand, a number of twin studies were carried out which did not confirm that PD was inherited, although they did not rule out that possibility

either [38, 39, 40]. A twin study by Tanner [41] in 1999 indicated that no genetic component contributes to PD when the age of onset is greater than or equal to 50 years, but there is a genetic contribution to PD beginning before this point.

1.2 The role of α-synuclein in Parkinson's disease

1.2.1 Early evidence

The plausibility of the genetic hypothesis was boosted by the discovery, in 1997, of a single mutation in a gene (which had been located on the long arm of human chromosome 4 a year before [42]) in a family known as the Contursi kindred, who lived in a town with the same name in the province of Salerno (Italy) and with a clinical picture typical of PD, although with a considerably lower onset age (46 ± 13 years) and with an autosomal dominant pattern of inheritance. The penetrance of the gene (that is, the proportion of family members showing the mutation that actually had the disease) was about 85 %, and the mutation was neither found in 314 chromosomes of unrelated individuals nor in 52 Italian patients with sporadic (non-familial) PD, strongly suggesting a causal relationship between the mutation and inherited PD. This gene is now called *SNCA* and encodes a protein known as *α-synuclein.* Sequencing techniques revealed the mutation to be a missense one in which the guanine at position 209 was substituted by an adenine (G209A), causing the Ala at position 53 of α-synuclein to be replaced by a Thr (A53T). It was the first time a particular point mutation was related to PD [43]. Shortly later, aggregates (mostly fibrils) of this protein were found to be (via immunochemical assays) the main component of Lewy bodies [44].

From this moment, α-synuclein attracted the attention of PD researchers and considerable efforts have been devoted to understanding its structure

and function since then. This protein had been first described in 1988 by Marotoux *et al.* [45], who had found a neuron-specific protein in *Torpedo californica* and rat, located both in the neurons' nucleus and in the synaptic terminals (that is why it was called *synuclein*) and, five years later, shown to be the precursor of the non-amyloid component (NAC) of the amyloid plaques characteristic of Alzheimer's disease [46, 47]. In 1995, the frequency of usage of the name "α-synuclein" in publications suddenly started rising (see figure 1.4). Since the 1997 key discoveries, a large number of further studies have demonstrated a connection between α-synuclein and the pathogenesis of PD, in both the familial and the more common sporadic form.
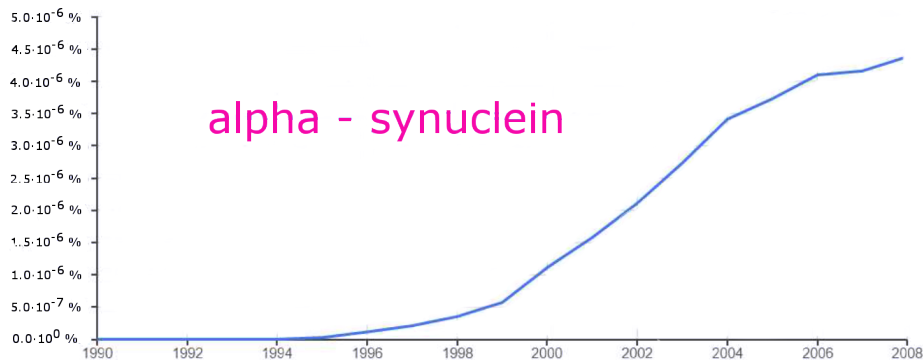
Figure 1.4: Evolution of the usage of the term "α-synuclein" from 1990 to 2008. Note the sudden increase taking place in 1995, two years after the protein was identified as the precursor of the non-amyloid component of Alzheimer's disease's amyloid fibrils. Generated with the *Google Books Ngram Viewer*. What the y-axis shows is the percentage of 3-grams (sets of 3 consecutive words) in a sample of books written in English and published in the United States within the period 1990-2008 matching "alpha-synuclein" (See Ref. [48] for details). Only data up to 2008 is available.

1.2.2 α-synuclein genetic alterations related to the disease

Besides the A53T mutation, a series of additional ones have been reported over the last two decades. Table 1.2 collects some data about each one of

them.

Table 1.2: Parkinson's disease-related human mutations known up to date. Nucl. subst. = nucleotide substitution in SNCA. AA subst. = aminoacid residue substitution in α-synuclein.

Year	Nucl. subst	AA subst.	Comments
1997	Guanine-adenine (G209A)	Ala-Thr (A53T)	The first PD-related mutation found, in the Contursi kindred [43]
1998	Guanine-cytosine (G88C)	Ala-Pro (A30P)	Found in a German family with Parkinson's disease [49]
2004	Guanine-adenine (G188A)	Glu-Lys (E46K)	Found in a Spanish family with Parkinson's disease and dementia with Lewy bodies [50]
2013	Guanine-adenine (G152A)	Gly-Asp (G51D)	Found in a French family with early-onset Parkinson's disease with implication of the pyramidal tracts (nerve fibers involved in motor control which travel from the cerebral cortex to the brain stem and to the spinal cord) [51]
2013	Thymine-guanine (T150G)	His-Gln (H50Q)	Related both to familial and sporadic Parkinson's disease with motor and non-motor symptoms [52, 53]
2014	Cytosine-adenine (C158A)	Ala-Glu (A53E)	Found in a Finnish female with early-onset, familial Parkinson's disease and multiple system atrophy, another α-synuclein-related neurodegenerative disease [54]

In addition to these missense point mutations, triplications [55] and duplications [56, 57] of SNCA have been associated to early-onset and later-onset PD, respectively. Additionally, upon comparison of duplication and triplication cases, it was observed that triplications correlate with a faster progression of the disease and with dementia and hallucinations, while duplications do with a slower progression and the absence of psychiatric conditions. This suggested a clear SNCA dosage effect on the severity of the disease.

Besides SNCA (also called "PARK1"), four additional genes have been related to parkinsonian hereditary disorders, namely leucine-rich repeat kinase

2 (LRRK2) (with unknown function), parkin or PARK2 (an enzyme which tags α-synuclein for degradation), P-TEN-induced putative kinase 1 (PINK1) (an enzyme which phosphorylates serines and threonines in response to oxidative stress) and DJ-1 or PARK7 (an antioxidant) [2]. The previously mentioned mutations are collected together and kept up to date in the *Parkinson disease Mutation Database* (PDmutDB) [2, 58, 59].

1.2.3 Structural properties of α-synuclein

1.2.3.1 Primary structure

α-synuclein is a relatively small protein (it only has 140 amino acid residues and a mass of 14 kDa), expressed in presynaptic terminals and either located in the cytoplasm or bound to the membrane. Its physiological functions are still not clear, but several possibilities have been proposed: synaptic vesicle recycling, synaptic plasticity or neurotransmitter synthesis and release [60]. On the basis of its primary structure, it is divided in three different domains:

- The N-terminal domain (residues 1-60): an amphipathic domain characterized by the presence of four 11-residue imperfect repeats containing a highly conserved 6-residue sequence: Lys, Thr, Lys, Glu, Gly (or Gln) and Val [KTKEG(Q)V]. This sequence is reminiscent of the α-helical domains of apolipoproteins (lipid-binding proteins) because of its characteristic periodicity of 11 [61].

- The non-amyloid component (NAC) (residues 61-95): with abundance of hydrophobic residues, two additional KTKEG(Q)V repeats and a 12-residue sequence (Val, Thr, Gly, Val, Thr, Ala, Val, Ala, Glu, Lys, Thr, Val, residues 71-82) that has been shown to be essential in the protein's aggregation [62]. Its name is due to the fact that it is, precisely, the aforementioned non-amyloid component of the amyloid plaques of Alzheimer's disease [47].

- The C-terminal region (residues 96-140): with a high concentration of negative charges (at physiological pH) and Pro, Asp and Glu residues.

1.2.3.2 Secondary structure

Concerning its secondary structure, spectroscopic and hydrodynamic studies [47] and replica exchange molecular dynamics (REMD) simulations [63] have shown that the protein must exist as an equilibrium mixture of several conformers with little or no organization (commonly called "random coil"). Depending on the surrounding medium, it may stay unfolded (in aqueous solution in physiological conditions) or adopt a partially folded conformation (when bounded to other molecules, or at low pH or high temperature), with α-helices or β-sheets, monomeric or oligomeric, or self-assemble into fibrils. Figure 1.5 depicts the primary and secondary structures of micelle-bound human α-synuclein (PDB code 1XQ8 [64]), and figure 1.6 shows a three-dimensional plot of its secondary structure. Because of its high conformational variability, it has been termed a "protein-chameleon" and characterized as a member of a protein family with similar structural properties. This family has been given different names in literature, taken from the Cartesian product of "natively, naturally, intrinsically" and "unfolded, unstructured, denatured" (see figure 1.7) [65].

In connection with this, many other proteins have been classified in this family and associated to diseases (e.g. tau protein, the main component of neurofibrillary tangles in Alzheimer's [67]) or found to be involved in essential regulatory biological functions, such as e.g. cell cycle control (which is the case of p21, a cycline-dependent kinase inhibitor) [68]. In these studies, it was observed that these proteins can interact with many different targets (precisely because of their unstructured nature) and that, upon these interactions, they adopt a (partially) ordered shape, just as α-synuclein does. The development of a number of protein disorder predictors [69, 70, 71] and their application to protein databases showed that lack of order is a conse-
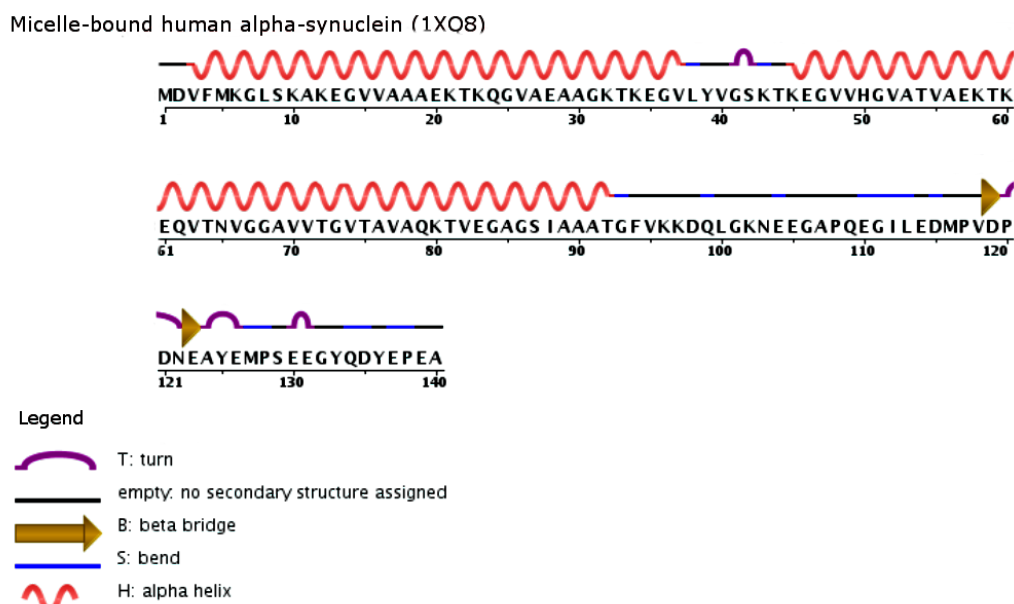
Figure 1.5: Primary and secondary structure of micelle-bound human α-synuclein (1XQ8). Note the α-helices at the N-terminal and the NAC regions, connected by a short turn, and the lack of secondary structure at the C-terminal domain. Modified from Ref. [66].

quence of a high net charge and an overall low hydrophobicity. Moreover, this kind of proteins turned out to be more abundant than thought, and a recent study proved that natural amino acid sequences are more disordered than randomly generated ones [72]. These facts have challenged the established view that a well-defined 3D structure is a necessary condition for a protein to be biologically functional.

Interestingly, despite this common belief that α-synuclein exists natively as an intrinsically disordered protein, it has been proposed that, actually, it shows a helically folded, stable tetrameric structure, on the basis of clear native polyacrylamide gel electrophoresis (CN-PAGE), scanning transmission electron microscopy (STEM), sedimentation equilibrium analytical ultracentrifugation (SE-AUC) and circular dichroism (CD) studies on α-synuclein extracted from human red blood cells [73]. This putative tetramer was subsequently found to be destabilized by the PD-related mutations A30P, E46K
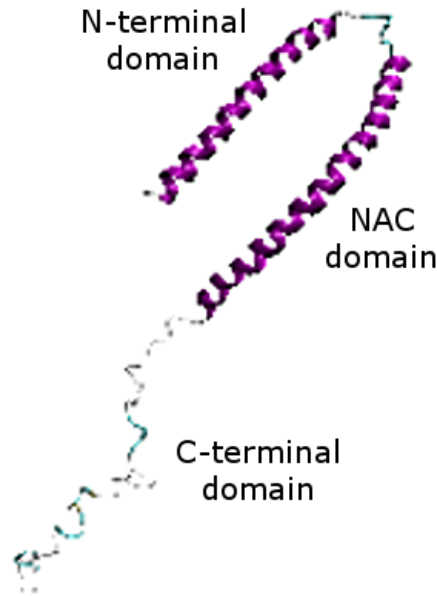
Figure 1.6: 3D representation of the secondary structure of micelle-bound human α-synuclein (1XQ8). Note again the α-helices at the N-terminal and the NAC regions, connected by a short turn, and the lack of secondary structure at the C-terminal domain.

and A53T [74] and conditioned to α-synuclein's N-terminal acetylation, a mild protein purification protocol and a high protein concentration [75]. Despite these findings, however, the unfolded monomer still seems to be the accepted α-synuclein native state [76].

1.2.3.3 Tertiary structure

Fibrils

Structure As mentioned earlier, α-synuclein fibrils are the major components of Lewy bodies, the intraneuronal hallmarks of PD. Much has been investigated with the aim of finding their molecular structure and a general

26

natively   naturally   intrinsically

unfolded   unstructured   denatured
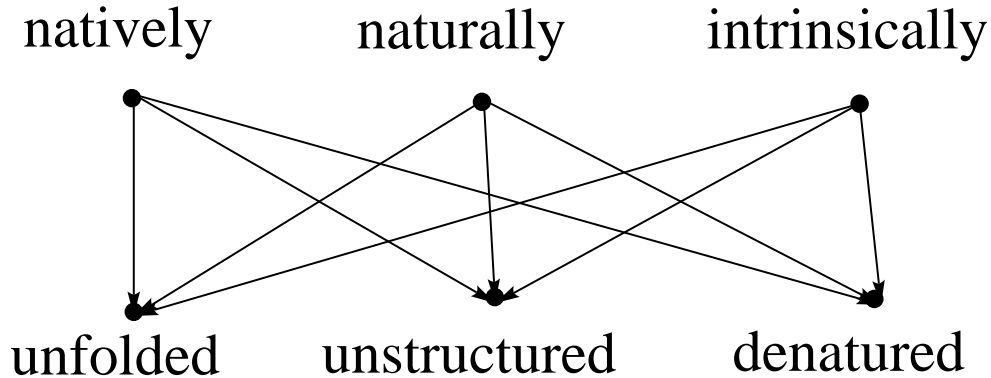
Figure 1.7: Representation of the different name combinations given to the α-synuclein protein family. Modified from Ref. [65].

mechanism by which certain proteins arrange into fibrils. In 2006, three general models were proposed: the "refolding" model, the "natively disordered" model and the "gain of interaction" model [77].

As for α-synuclein, the structure of its fibrils has been studied by means of CD measurements, X-ray and electron diffraction experiments [78], observing that they had a CD spectrum typical of β-sheet rich structures and cross-β diffraction patterns characteristic of amyloid fibrils. Immunoelectron microscopy was also applied in this study, revealing that the C-terminal region was exposed on the fibrils' surface and, therefore, the N-terminal one was buried.

Other techniques, like quenched hydrogen/deuterium exchange nuclear magnetic resonance (NMR) spectroscopy, have been applied to the determination of the precise location of these β-sheets in the protein's sequence [79], leading to the identification of five putative β-strands comprising (approximately) residues 35-41, 49-56, 60-67, 69-82 and 86-94 (mainly in the NAC domain), while residues 1-27 and 104-140 were found not to be included in the secondary structured regions. The location of these five β-strands was confirmed in the same study by means of solid-state NMR experiments, which additionally showed that they were spatially arranged in a five-

layered "β-sandwich". Furthermore, high-resolution cryoelectron microscopy allowed the observation of both straight and twisted α-synuclein fibrils (see figure 1.8b). Remarkably, a recent computational study in which a simplified coarse-grained (CG) model was used to represent α-synuclein monomers, yielded these same conclusions about the localization of the residues involved in the fibrillation process [80].

(a)

(b)
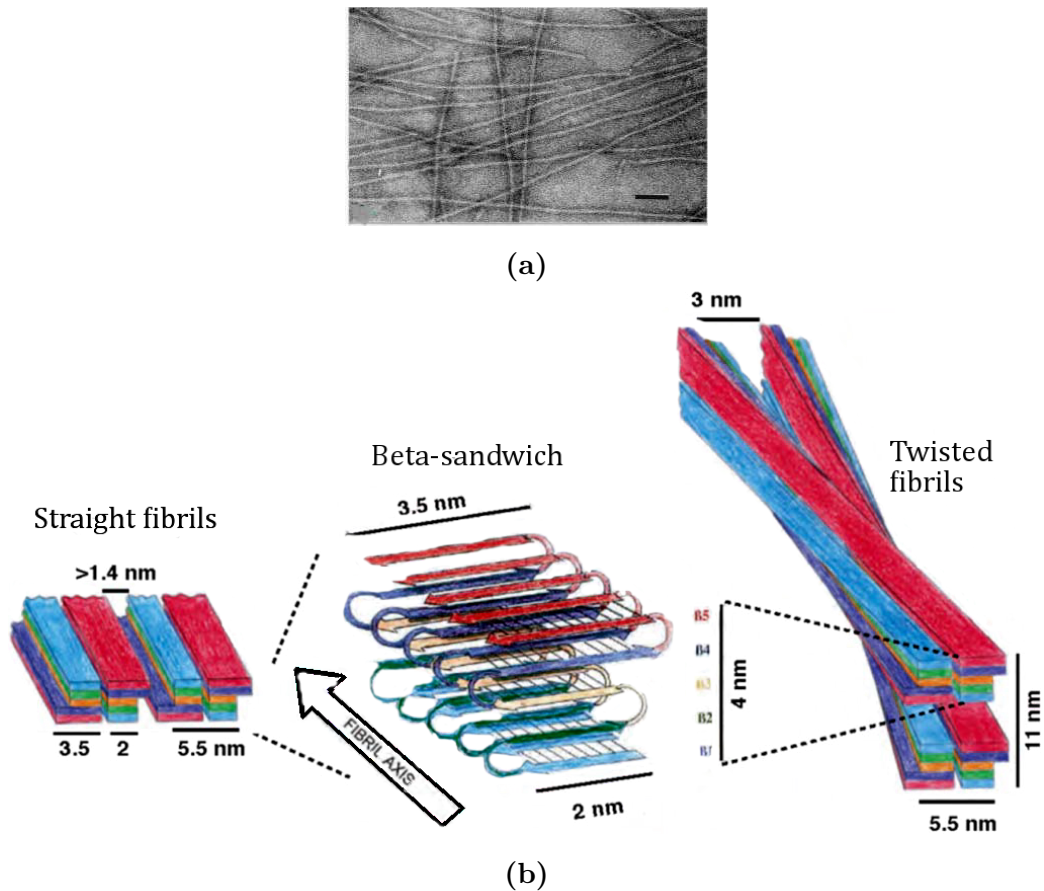
Figure 1.8: (a): Morphology of α-synuclein fibrils, as revealed by electron microscopy. Scale bar, 100 nm. Modified from Ref. [78] (b): Representation of the spatial arrangement of straight and twisted α-synuclein fibrils, with the underlying five-layered β-sandwich. Modified from Ref. [79]

Kinetics of formation   α-synuclein's aggregation mechanism has been shown to produce a sigmoidal profile (implying it is nucleation-driven) and to

proceed through α-helical oligomeric intermediates [81, 82]. In 2008, Bharathi and coworkers proposed, for the first time, an empirical mathematical model to describe the aggregation kinetics of α-synuclein [83] showing that it comprises a lag, a growth and a stationary phase (see figure 1.9) and highlighting the importance of the role played by the oligomeric species.
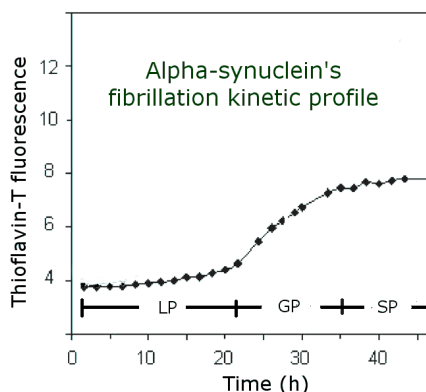
Figure 1.9: Sigmoidal curve describing a nucleation-driven fibrillation kinetics, characteristic of α-synuclein. The lag, growth and stationary phases (LP, GP and SP, respectively) are indicated. Adapted from Ref. [83].

Alterations in α-synuclein primary structure have been determined to have an effect on its aggregation rates. As an example, a recent CG MD study suggested that A30P and A53T α-synuclein inhibited the formation of a transient β-hairpin (putatively a key event in the protein's self-assembly) in the 38-53 region, in comparison with the wild-type (unaltered) protein, thereby delaying its aggregation [84].

Oligomers: the precursors of fibrils The fact that fully formed α-synuclein fibrils are the major components of Lewy bodies led to the idea that they were the PD-associated cytotoxic species. Nevertheless, there is substantial evidence suggesting not only a link between prefibrillar aggregates (oligomers) and PD pathogenesis, but also the nonexistence of a critical role of mature fibrils in it. In particular, there is no correlation between the presence of fibrils (Lewy bodies) in PD brains and signs of neuronal death [85],

some animal models show PD-like phenotypes before fibrils can be detected [86], *in vitro* formation of these oligomeric species (unlike the monomeric and fibrillar ones) disrupts vesicle membranes [87] and *in vivo* studies have directly confirmed that α-synuclein oligomers cause dopaminergic loss and disrupt cell membranes more than fibrils do [88].

Some artificial α-synuclein mutants have shown a tendency not to form fibrils, but oligomers. These include E35K and E57K. However, all known familial PD-related mutants end up forming fibrils (although at different rates, as explained above). The toxicity of these α-synuclein oligomeric forms has been associated to their different shapes, which have been studied through a variety of experimental techniques, including Raman spectroscopy, atomic force microscopy (AFM) [89], CD, Fourier transform infrared spectroscopy (FTIR), size-exclusion chromatography (SEC), high-performance liquid chromatography (HPLC) or small-angle X-ray scattering (SAXS) [90]. The early-stage oligomers have globule-like spheroidal shapes, while the late-stage ones consist of chained spheroids (commonly referred to as protofibrils).

A third structurally distinct class of oligomers, characterized by a ring shape, has also been described [91]. MD studies suggested that the formation of these oligomers is favored by the previous formation of propagating dimers that bind to the cell membranes and facilitate the incorporation of more monomers [92], and they have been proposed to mediate neurotoxicity by a pore-like mechanism [93]. However, this view has been challenged [94], so the pathological significance of these species is not entirely clear.

1.2.4 Factors altering the structure of α-synuclein

1.2.4.1 Interactions with other (bio)molecules

Besides interacting with itself, α-synuclein shows affinity for several hundred other biomolecules. More precisely, an extensive proteomics study [95] found

324 proteins interacting with it, including tubulin (the main constituent of cytoskeleton) or calmodulin (a multifunctional calcium-binding protein). α-synuclein is also known to bind DNA [96], β and γ-synucleins [97], and chaperons (proteins that refold other proteins) like torsin A [98], heat-shock protein 104 [99] or αβ-crystallin [100]. More recent studies have detected additional molecules, such as the flavonoids quercetin [101] and clioquinol [102], rotenone [103] or the peptidyl prolyl isomerase FKBP12 [104]. Moreover, a computer-aided drug design (CADD) study employing MD simulations as well as docking-scoring techniques found out that the steroid stimovul might bind to Ser 87 and Val 95 [105]. Some of these molecules were seen to enhance α-synuclein aggregation (rotenone, FKBP12) and some others, to attenuate it (β and γ-synucleins, chaperons, flavonoids). These effects were all related to the induction of conformational changes in α-synuclein.

The properties of α-synuclein related to its aggregation (spatial conformation, charge, hydrophobicity) are affected not only by the presence of point mutations, its overexpression due to gene multiplications or its combinations with other molecules, but also by side chain alterations, such as the so called "posttranslational modifications" (PTMs), by environmental factors, such as its interactions with (heavy) metals, or by an interplay of all of them. In the next two subsections, these factors are explained in more detail.

1.2.4.2   Posttranslational modifications

More than 300 PTMs have been described for proteins [106]. α-synuclein is susceptible to a subset which includes, but is not limited to, phosphorylation, nitration, oxidation, glycation and N-terminal acetylation.

Phosphorylation   Phosphorylation was the first α-synuclein PTM to be discovered, and the most extensively studied one. A major phosphorylation site, Ser 129, has been described for α-synuclein [107]. Two secondary sites, Ser 87 [108] and Tyr 125 [109], have also been established. Phosphorylation

at Ser 129 was found to promote aggregation *in vivo*, and its substitution by an Ala residue was found to inhibit this process [110]. Furthermore, it has been determined that about 90 % of α-synuclein present in Lewy bodies from PD patients is phosphorylated at site 129, while this is only the case in around 4 % (at most) of it in controls [111], providing strong evidence for its implication in the etiology of the disease. However, phosphorylation at the other two sites were seen to block α-synuclein's conversion into toxic species [112], suggesting that an imbalance between phosphorylation at Ser 129 and at the other positions may lie at the origin of PD.

Nitration Nitrative and oxidative stresses are generally believed to be implicated in neurodegeneration. Nitrated forms of α-synuclein were detected on PD, DLB, the Lewy body variant of Alzheimer's disease and MSA brain tissue samples by means of immunohistochemical analyses, which also allowed to determine that the targets of nitration were the four Tyr residues (at positions 39, 125, 133 and 136) [113]. Previously, the formation of 3-nitrotyrosine (3-NT) in both human disease and *in vitro* and *in vivo* models and the implication of nitric oxide-derived and reactive oxygen species (ROS) in it had been reported [114]. The exposure of recombinant human α-synuclein to potential *in vivo* nitrating agents was shown to nitrate the four Tyr residues of α-synuclein, and also to yield very stable dimers and higher order oligomers [115]. This was interpreted as the generation of α-synuclein o,o'-dityrosine crosslinks. Figure 1.10 depicts the free-radical pathways leading to the formation of both 3-NT and crosslinked dityrosine.
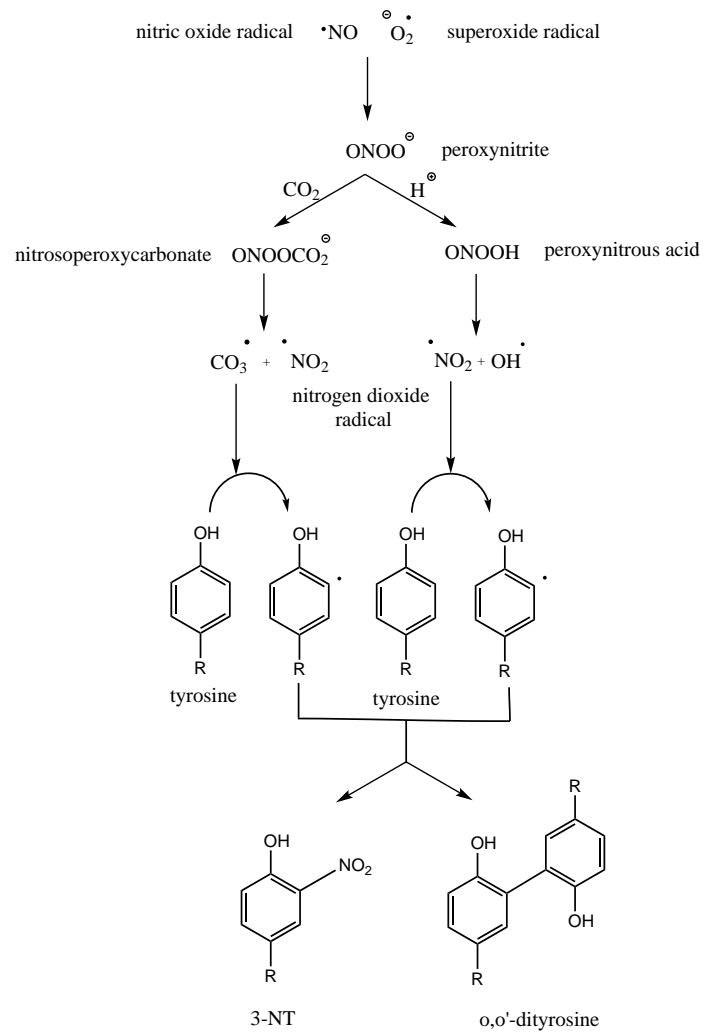
Figure 1.10: Free-radical pathways leading from nitric oxide and superoxide to 3-NT and o,o'-dityrosine crosslinks. Note the involvement of highly reactive species such as peroxynitrite or nitrogen dioxide. Adapted from Ref. [116].

Oxidation Oxidative α-synuclein modifications can affect Met residues (located at positions 1, 5, 116 and 127), turning them into sulfoxides. FTIR and CD studies of H_2O_2-oxidized α-synuclein suggested that, at neutral pH (but not at acidic one), it had a smaller content of β-structure and a higher degree of disorder with respect to the native (non-modified) protein, which was attributed to its higher polarity. Also, it had a lower tendency to form fibrils and inhibited the fibrillation of the native protein by stabilizing non-toxic oligomers, with the extent of this inhibition being directly proportional to the number of oxidized Met residues [117]. It was proposed that α-synuclein's Met residues' oxidation (and subsequent reduction mediated by methionine sulfoxide reductase) may protect other cellular components from ROS [118]. However, a recent study [119] provided evidence for the prominent role of methionine 5 UV-induced oxidation in the formation of α-synuclein toxic oligomers. In light of these studies, methionine oxidations influence α-synuclein's structure and fibrillation properties, promoting the formation of mostly non-toxic oligomers, perhaps with the exception of methionine 5.

Glycation The fact that α-synuclein has 15 Lys residues in its primary sequence makes it an ideal target for glycation. This reaction, also known as the Maillard reaction, implies the non-enzymatic binding of an amino (or thiol) group to a carbonyl group of a reducing sugar or a sugar or lipid-derived aldehyde, resulting in a Schiff's base, which subsequently undergoes a rearrangement (known as the "Amadori rearrangement"), leading to a ketoamine called the "Amadori product". This intermediate compound evolves, through a variety of reactions (including oxidations, dehydrations, condensations, fragmentations or cyclizations), towards a heterogenous set of products known as *advanced glycation end products* (AGEs), generating ROS as byproducts (see figure 1.11) [120]. Proteins can undergo this PTM by reacting through the amino group of their Lys or Arg residues or through the thiol group of their Cys residues [121]. In particular, all α-synuclein's Lys residues are candidates for glycation and ulterior AGEs formation [122].

Abnormally high amounts of two common AGEs, namely pentosidine and pyrroline, were found in Lewy bodies from the substantia nigra of PD brains [123]. AGEs were also detected in healthy brains, although in much lower levels, and AGE receptors (RAGEs), which bind AGEs initiating a cascade of deleterious events, were also present in both the substantia nigra and the cerebral cortex in patients with early parkinsonism, in much higher amounts than in controls [124]. Moreover, two of the most common *in vivo* glycating agents, namely the dicarbonyl compounds glyoxal and methylglyoxal, were found to inhibit α-synuclein fibrillation *in vitro*, stabilizing potentially toxic oligomers [125]. Taken together, these results seem to point to a relation between AGEs and oxidative stress which might be relevant to neurodegeneration.
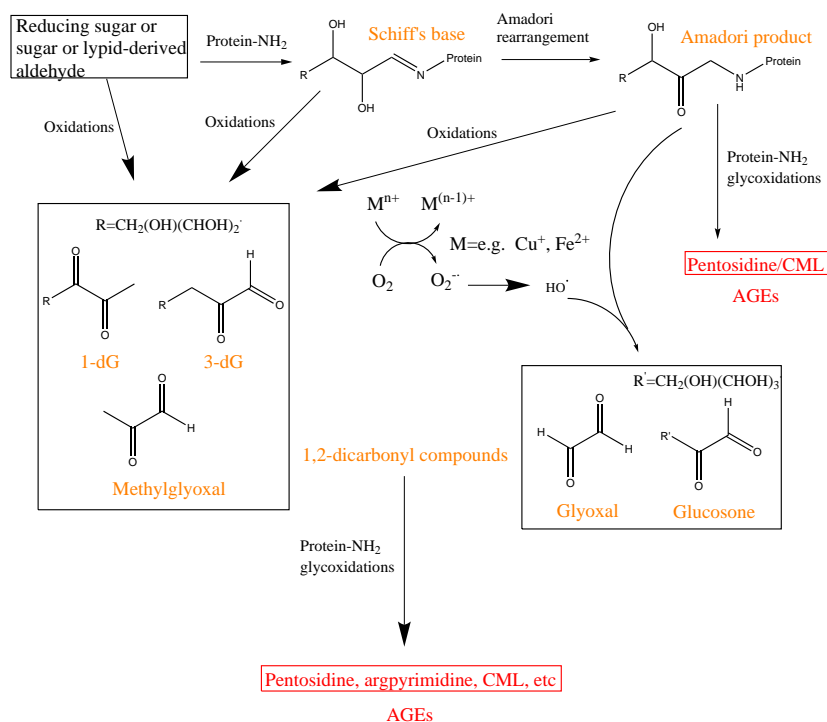
Figure 1.11: Molecular pathways leading to AGEs formation. Note that sugars or aldehydes may be directly oxidized into highly reactive dicarbonyl compounds, in addition to forming the Amadori product and evolving from there. Adapted from Ref. [126].

N-terminal acetylation Protein N-terminal acetylation is a ubiquitous PTM in eukaryotes (but not in bacteria), and it is catalyzed by the N-acetyltransferase (Nat) family of enzymes: NatA, NatB and NatC [127]. Each one of these three proteins binds selectively to specific N-terminal sequences, with NatB acting on methionine-aspartate and methionine-glutamate termini [128], the former corresponding to the α-synuclein one. In this protein, N-terminal acetylation has been proposed to be essential for its binding to the membrane, since e.g. inhibition of NatB activity (but not of NatA or NatC) in yeast cells caused the protein cell distribution to shift towards the cytoplasm [129], and it has been widely detected in both diseased an healthy individuals [111]. N-terminal acetylation of both recombinant and semisynthetic α-synuclein did not seem to affect its large-scale conformation or its monomeric state, on the basis of CD and NMR studies [130], but there was a considerable gain of α-helical structure at the N-terminus which extended up to residue 12 [131]. Moreover, the aggregation and fibrillation rates of N-terminal acetylated α-synuclein were slower than those of the unmodified protein [132]. These results indicate that this PTM does not play a significant role in α-synuclein toxicity but that it may be physiologically relevant by inducing its binding to membranes.

1.2.4.3 Interactions with (heavy) metals

Generalities The positive correlation between long-term exposure to heavy metals and PD has long been known, and has been demonstrated in a large number of epidemiological studies [133, 134, 135], postmortem analyses of PD brains [136, 137] and *in vivo* studies [138], with copper, iron, manganese, aluminum, lead and zinc being the main metals identified. The effect of metal cations on α-synuclein structure and fibril formation has also been established *in vitro* as well as *in vivo*. In a study conducted by Uversky and others in 2001 [139], a systematic analysis of the influence of a set of metal cations on α-synuclein aggregation rates and structure was performed, show-

ing a correlation between the metal charge densities (charges per unit ionic volume) and their ability to enhance these properties. Accordingly, trivalent and divalent cations (such as Al^{3+}, Fe^{3+}, Co^{3+} or Cu^{2+}, but not Mg^{2+} or Ca^{2+}) increased aggregation rates and induced secondary structure, whereas monovalent cations did not have any significant effects. It was proposed that active metals neutralized the negative charges, reducing intramolecular electrostatic repulsion and stabilizing a partially folded conformation, thereby enhancing aggregation. In this study, Al^{3+} was recognized as the most effective ion to induce intramolecular structural changes in α-synuclein and to accelerate its aggregation.

Copper Cu^{2+} is the most studied metal cation in relation to α-synuclein. This protein, both recombinant and overexpressed in cells, has been identified as a Cu^{2+}-dependent ferrireductase. Fe^{2+} is known to be necessary for tyrosine hydroxylase, an enzyme involved in the synthesis of dopamine, whose levels can therefore be depleted when Fe^{2+} is not abundant. What is more, Fe^{3+} can induce the formation of ROS, resulting in cell death [140]. This was the first direct observation of a dopamine-related physiological function in α-synuclein.

The Cu^{2+}-α-synuclein binding sites have been the object of many studies. As an example, Sung and coworkers [141] used NMR to map a number of them at the C-terminal region (centered at Asp 121) and a few ones at the N-terminus, particularly the amino group of Met 1 and the imidazole ring of Hie 50. N-terminal binding sites were identified as high-affinity ones (in the sense that they required relatively low concentrations of Cu^{2+} to achieve a complete broadening of the NMR signal), while C-terminal ones were determined to be low-affinity sites. In this study, Met 1 and Hie 50 were found to be independent binding sites, since the substitution of the latter with an alanine did not inhibit the binding to the former. In contrast with this, other studies [142, 143] have found that, in fact, there is a single site involving both residues. A recent study by De Ricco [144] reported, however,

that the residues involved in Cu^{2+} complexation depended on the pH and the relative concentrations of Cu^{2+} and protein: at low pH, His 50 did not participate, at high pH and low relative Cu^{2+} concentration, Hie 50 did, and at high pH and high relative Cu^{2+} concentration, a second coordination site around Hie 50 coexisted with the one around Met 1. Interestingly, Cu^{+} did not bind Hie 50, but the side chains of Met residues [145].

Overall, Cu^{2+} may play a role in α-synuclein function and shows a high number of putative coordination sites.

Iron   The connection between iron and α-synuclein has also been addressed. Fe^{2+} has been seen to contribute to disease both by promoting its aggregation and by the generation of ROS (hydrogen peroxide and hydroxyl radical) by Fenton's reaction [146], although a decrease in its concentration (and a concomitant increase in Fe^{3+}) has been reported in PD brains [136]. This fact may be related to the already mentioned ferrireductase activity attributed to α-synuclein. A single low-affinity binding site located at the Asp 121-Asn 122-Glu 123 region has been assigned to Fe^{2+} [147] and this complex was shown to be oxidized in the presence of oxygen, with generation of hydrogen peroxide [148].

Zinc   It has been determined that Zn^{2+} binds to α-synuclein as well. Despite the abundant studies showing the stimulatory effect of this metal cation on α-synuclein's fibrillation, it was not until 2012 when its binding sites and the structure of its complexes were addressed [149]. By using NMR spectroscopy, it was concluded that Zn^{2+} had a strong preference for Asp 121 and a weaker one for Hie 50 and some undetermined secondary sites at the C-terminal region, all of them being independent sites. Interestingly, the binding affinities were found to be in the millimolar range, whereas the usual Zn^{2+} concentrations *in vivo* are in the nanomolar range, thus challenging the physiological relevance of α-synuclein-Zn^{2+} complexes.

Aluminum Al^{3+} was determined to induce a considerable modification of α-synuclein secondary structure, since it caused drastic changes to its CD and UV absorbance spectra and increased its intrinsic fluorescence more than other metal cations did [139]. These effects were attributed to the Al^{3+}-induced alteration of the environment of the fluorescent Tyr residues and to the binding of Al^{3+} to fluorescence-quenching undetermined carboxylate groups lying close to them.

1.3 Graphical summary

Figure 1.12 schematically represents the four categories in which factors affecting α-synuclein's aggregation could be classified. As it can be inferred from the ideas exposed, the interplay between all of them lies at the origin of neurodegeneration, but the precise way in which they interact is by no means completely understood. That is why in-depth studies in this area are still necessary.
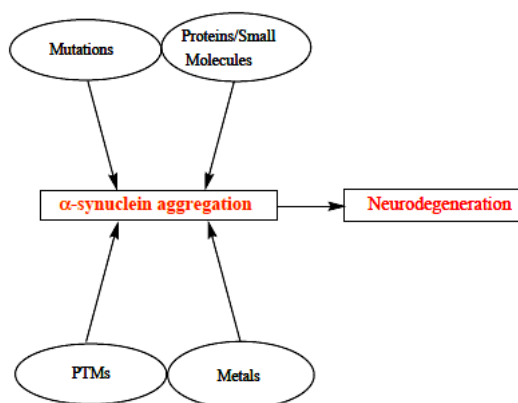
Figure 1.12: Factors influencing α-synuclein structure and accelerating (or inhibiting) its aggregation and fibrillation. They can be both genetic and environmental, although a combination of both is prevalent. Adapted from Ref. [96].

Chapter 2

Methodology

2.1   Aim

The aim of this work was to carry out a computational study on the formation of coordination complexes between α-synuclein and (heavy) metals (some of them experimentally found and some others proposed here) in order to characterize the equilibrium geometries of the (putative) binding sites, to estimate their relative thermodynamic stabilities and to study the bond formation between the metals and α-synuclein dipeptide model systems.

For this, a series of chelates involving a dipeptide consisting of two consecutive residues in α-synuclein's primary sequence, a central metal cation and possibly a water molecule, and having the form depicted in figure 2.1, have been built and their geometries optimized. Subsequently, a vibrational analysis has been performed for each complex, in order to characterize them as true minima, and to compute an estimation of their Gibbs free energies at 298.15 K and 1 atm. The effect of the solvent (water) has been taken into account by using an implicit solvent model. This whole procedure has been repeated for the ligands (the dipeptides) alone, for the metal cations coordinated to six explicit water molecules and for the water molecule alone,

so that the following equation:

$$\text{Metal}(\text{H}_2\text{O})_6 + \text{Ligand(s)} \rightarrow \text{Complex} + n\ \text{H}_2\text{O}, \quad n \in \{5, 6\}$$
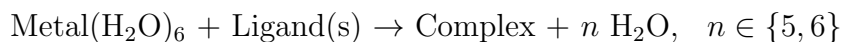
could be used as a working reaction to compute free energy differences. After this, an analysis of the topology of the electron density by applying Bader's theory of atoms in molecules (AIM) [150], as well as a natural bonding orbital (NBO) population analysis [151], have been used to try to understand the nature of the bonds between the cations and the dipeptides.

As stated in the *Introduction* chapter, Cu is the most widely studied α-synuclein-binding transition metal, and in particular Cu^{2+} is the cation for which the largest number of possible coordination sites have been proposed. Also, Zn^{2+} has been found to associate with α-synuclein at a number of sites (although some of them undetermined or with especially low affinity) and to substantially increase its fibrillation rates, while Al^{3+} was the cation inducing the most drastic intramolecular changes due to its highest charge density [139]. Regarding the complexes' geometries, Cu^{2+} has been proposed to form square planar (or distorted tetragonal) chelates [152], but no data could be found for Zn^{2+} or Al^{3+}. In order to compare and contrast these experimental findings with a theoretical prediction, these three cations have been selected for this study.

Table 2.1 shows the list of the studied complexes, which include the experimentally proposed high-affinity sites for Cu^{2+} involving Met 1, Asp 2 and Hie 50 and the low-affinity one at the Asp 121-Asn 122 region (so as to compare results and validate the methodology used here), and some analogous ones involving either an Asp, a Ser or a Thr as the anchoring site, two deprotonated backbone amide functions and a water molecule to complete the coordination sphere. Each complex was optimized first with Cu^{2+}. Then, the cation was removed and the ligand reoptimized (to obtain the isolated ligands) or the cation was substituted with Zn^{2+} or Al^{3+} and the

complex reoptimized (to obtain the complexes with these two cations). Asp, Ser and Thr were chosen as the anchoring sites since they have a charged or nucleophilic group that could potentially bind the cation (see figure 2.2 for their chemical structures) and their side chains are 2 or 3 atoms long, thereby allowing a near square planar geometry for the complexes. As for the backbone amides, it has been suggested that, although they usually have a considerably high pKa value, their deprotonation is favored when a metal cation binds to a neighbor side chain in chelating position with the amide nitrogen [153].
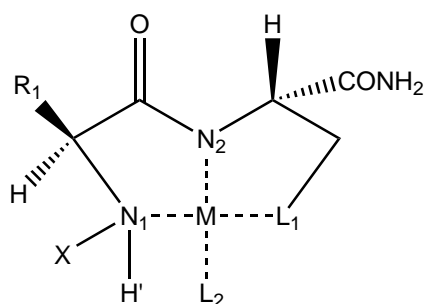
Figure 2.1: Common structure for all the complexes studied. M is Cu^{2+}, Zn^{2+} or Al^{3+}. L_1 is the charged or polar group in the side chain of an aspartate, a serine or a threonine. R_1 are the side chains of the residues appearing one position before the ones containing L_1 in α-synuclein's primary structure. L_2 is always a water molecule except for complexes 3, 4, 5 and 6, in which it is the ε or δ nitrogen of the imidazole ring of an Hid or Hie. X is always an acetyl group, except for complex number 1, in which it is a hydrogen. H' is only present in complex 1 and it also represents a hydrogen.
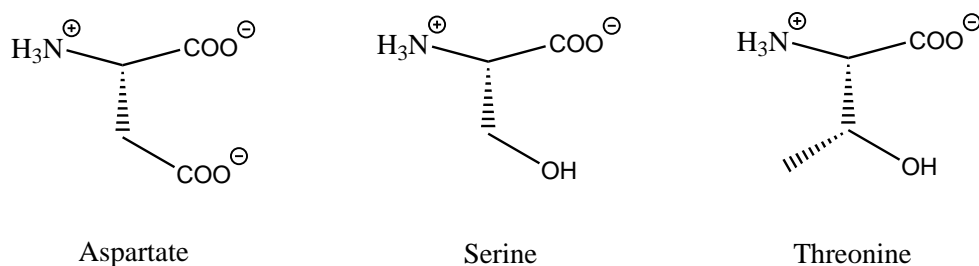
Figure 2.2: Chemical structures of Asp, Ser and Thr, the selected anchoring sites.

Table 2.1: List of complexes studied, each one with Cu^{2+}, Zn^{2+} and Al^{3+}. The horizontal lines mark the limits of the three α-synuclein domains. Experimentally found sites are written in blue, while sites proposed in this work are shown in orange. No. = site number. α-syn seq. = position in α-synuclein sequence. R_1 res. = residue bearing R_1. L_1 res. = residue bearing L_1.

No.	α-syn seq.	R_1 res.	L_1 res.	L_2
1	1-2	Met	Asp	H_2O
2	1-2	NacMet	Asp	H_2O
3	1-2-50	Met	Asp	Hid
4	1-2-50	NacMet	Asp	Hid
5	1-2-50	Met	Asp	Hie
6	1-2-50	NacMet	Asp	Hie
7	8-9	Leu	Ser	H_2O
8	41-42	Gly	Ser	H_2O
9	43-44	Lys	Thr	H_2O
10	49-50	Val	Hie	H_2O
11	53-54	Ala	Thr	H_2O
12	74-75	Val	Thr	H_2O
13	97-98	Lys	Asp	H_2O
14	114-115	Glu	Asp	H_2O
15	118-119	Val	Asp	H_2O
16	121-122	Asp	Asn	H_2O
17	134-135	Gln	Asp	H_2O

2.2 Computational details

Kohn-Sham Density Functional Theory (KS-DFT) has been the selected theoretical method for this study. Specifically, the M06 functional, developed by Zhao and Truhlar [154] combined with the 6-311+G(d,p) basis set and the Solvation Model Density (SMD) implicit solvation model [155], has been used throughout. Furthermore, in order to assess the magnitude of the dispersion effects on the complexes' geometries and energies, the M06 results have been compared with those obtained with the dispersion-corrected ωB97X-D functional, developed by Chai and Head-Gordon [156], while using the same basis functions and implicit solvation model. Since Cu^{2+} complexes are open-shell systems, the unrestricted formalism has been applied in all the calculations (even in the ones involving Zn^{2+} complexes, and in the isolated ligands or the water molecules, although these are closed-shell systems). All optimizations and NBO calculations have been performed with the Gaussian 09, Revision B.01 computational chemistry software [157] (which includes the NBO program in its 3.1 version [158]), and the Multiwfn 3.3.7 software [159] has been used for the AIM analysis.

2.2.1 Density functionals

2.2.1.1 M06

M06 is a hybrid meta-generalized gradient approximation (MGGA) exchange-correlation functional containing a 27 % of Hartree-Fock (HF) exchange. It showed the best performance in predicting reaction energies of transition metal-containing systems when tested against other 13 functionals not including a 100 % of HF exchange (the ones which do, such as M06-HF or HFLYP, are known not to be suitable for transition-metal chemistry), so it was recommended by its designers for this kind of problems [154]. Furthermore, a number of DFT studies on the thermodynamics of transition metal

complexes have employed this functional in the recent years [160, 161, 162].

2.2.1.2 ωB97X-D

ωB97X-D is one of the so called DFT-D functionals, which are the sum of a KS-DFT contribution and an empirical atom-atom correction for long-range van der Waals interactions, thereby including this effect without any extra computational cost:

$$E_{DFT-D} = E_{KS-DFT} + E_{disp}$$

In the case of ωB97X-D, the KS part E_{KS-DFT} is the ωB97X functional (which is one of the so called long-range corrected (LC) hybrid functionals, with a 15.8 % of short-range HF exchange and full long-range HF exchange) [163] and the empirical part is given by:

$$E_{disp} = - \sum_{i=1}^{N_{at}-1} \sum_{j=i+1}^{N_{at}} \frac{C_6^{ij}}{R_{ij}^6} f_{damp}(R_{ij})$$

with the damping function f_{damp} given by:

$$f_{damp}(R_{ij}) = \frac{1}{1 + a(R_{ij}/R_r)^{-12}}$$

where N_{at} is the number of atoms, R_{ij} is the distance between atoms i and j, R_r is the sum of van der Waals radii of atoms i and j and a is a parameter determining the strength of dispersion corrections [156].

This approach follows the Grimme's method for computing dispersion corrections [164] except for a different damping function, which in Grimme's work is:

$$f_{damp}(R_{ij}) = \frac{1}{1 + e^{-d(R_{ij}/R_r-1)}}$$

and the fact that the dispersion energy is not scaled. The ωB97X-D functional was proven to be generally better than other DFT-D functionals like B97-D, B3LYP-D or BLYP-D [156].

2.2.2 SMD implicit solvation model

Implicit solvation models treat the solvent as a continuum medium and the solute as a charge distribution inside a cavity that separates it from the solvent. They add a term to the energy of the solute that represents its solvation free energy, which is generally expressed as the sum of an electrostatic and a non-electrostatic (cavitation, dispersion and solvent structural effects) contribution. In the SMD model, the electrostatic part is computed from the reaction field (the electrostatic potential due to the interaction between the solute and the solvent), which is itself obtained by self-consistently solving the nonhomogeneous Poisson equation (which depends parametrically on the solvent's dielectric constant and the solute's charge density) with the Integral Equation Formalism Polarizable Continuum Model (IEF-PCM) algorithm [165], whereas the non-electrostatic term depends on the solute's solvent-exposed surface area and on solvent descriptors such as the refractive index or acidity and basicity parameters. SMD does not approximate the solute's charge density with distributed point charges or multipoles (it uses the continuous charge density instead), so its accuracy does not rely on the ability of a given level of theory to compute suitable partial atomic charges. In its original paper, SMD was seen to outperform the default Gaussian 03 IEF-PCM model and the default algorithm for computation of non-electrostatic terms [155], and it is also recommended by the Gaussian 09 User's Reference [166].

2.2.3 Thermochemistry

In Gaussian, thermochemical data (internal thermal energies, enthalpies, entropies and Gibbs free energies) are computed as the sum of the contributions from translational, rotational, vibrational and electronic partition functions, using the standard equations from statistical mechanics [167]. The thermal energy (and the enthalpy and Gibbs free energy calculated from it) includes the zero point vibrational energy. Gibbs free energies of formation of the complexes (ΔG_f) in this work have been obtained as the difference between the Gibbs free energies of products and reactants in the working reaction presented in section 2.1.

2.2.4 Atoms in molecules (AIM) theory

The Bader's theory of atoms in molecules [150] is based on the study of the topology of the electron density $\rho(x, y, z)$ (its gradient, its critical points and the eigenvalues of its Hessian matrix at them) to define atoms, bonds, rings and cages in a molecule.

Critical points of ρ are those at which its gradient vanishes. The rank ω of a critical point r_0 is the number of non-negative eigenvalues of the Hessian matrix of ρ at r_0, and its signature s is the algebraic sum of the signs of its eigenvalues. A critical point is identified with the pair (ω,s). Critical points of rank 3 are indicative of a stable structure. According to their signature, critical points are classified as:

- (3,-3): with three negative eigenvalues, they are local maxima of ρ and are found at the nuclei positions.

- (3,-1): with two negative eigenvalues, they are maxima of ρ on the plane determined by the two corresponding eigenvectors and minima along the direction perpendicular to it. They are called *bond critical points*.

- (3,+1): with two positive eigenvalues, they are minima of ρ on the plane determined by the two corresponding eigenvectors and maxima along the perpendicular direction. They are called *ring critical points*

- (3,+3): with three positive eigenvalues, they are local minima of ρ, and are called *cage critical points*.

In this theory, the definition of atoms is based on the gradient vector field of ρ. A gradient path is a line obtained by following the gradient of ρ, in small steps, starting at any point. Surfaces in three-dimensional space that are not traversed by any gradient path (zero-flux surfaces) are called *interatomic surfaces*, and the regions they determine are called *atomic basins*. Inside each atomic basin, all gradient paths terminate at the same point (a nucleus), and an atom is defined as the union of the nucleus and its basin.

Neighboring basins may be connected by a line such that, at each of its points, ρ is maximum along directions perpendicular to the line. This line is called a *bond path*. The molecular graph for a given molecule has the nuclei as vertices and the bond paths as edges. This molecular graph generally coincides with the molecular connectivity obtained on the basis of chemical considerations, and it works for covalent as well as non-covalent interactions.

While the value of ρ at a bond critical point gives an idea of the bond strength, the sign of the Laplacian of the electron density, $\nabla^2\rho$, at that point is related to the nature of the bond. A negative value of $\nabla^2\rho$ indicates that the electron density is higher at the point than in a neighborhood of it (so electron density is locally concentrated, an indication of a covalent bond). A positive value of $\nabla^2\rho$ indicates that the electron density is lower at the point than in a neighborhood of it (so electron density is locally depleted, an indication of a non-covalent bond). Therefore, the AIM theory is useful to confirm the presence of non-covalent interactions in a molecule, as well as other molecular structure elements such as rings or cages.

2.2.5 Natural bond orbitals

Natural bond orbital (NBO) analysis [151] provides an intuitive picture of chemical bonding by expressing the electron density computed from DFT or wave function methods in terms of localized electrons and lone pairs, as in a Lewis structure. To do so, it relies on a set of orbitals different from the canonical one, called natural atomic orbitals (NAOs). By definition, canonical orbitals are the eigenfunctions of the Fock matrix, while NAOs are orthonormalized eigenfunctions of certain submatrices of the density matrix, each one of which consists of the rows and columns of the full matrix corresponding to the basis functions centered on a particular atom in the molecule. The associated eigenvalues are called the occupancies. The best approximation (in a least-square sense) of the electron density as a linear combination of orthonormal functions is obtained by choosing the NAOs as the functions and the corresponding occupancies as the coefficients.

In Gaussian 09, once the NAOs are computed, those with an occupancy greater than 1.99 are termed *core orbitals*, and those with an occupancy larger than 1.90 are called *lone pairs*. Then, a search is carried out over two-atom submatrices of the density matrix, looking for eigenvectors with occupancies greater than 1.90. These eigenvectors are the *natural bonding orbitals* (NBOs), which can be expressed as linear combinations of *natural hybrid orbitals* (NHOs), which are, in turn, linear combinations of NAOs on the corresponding atoms. The 1.90 threshold is lowered if the sum of the occupancies of the identified orbitals differs by more than one unit from the total number of electrons. The search for lone pairs and NBOs is repeated looking for eigenvectors with occupancies less than 0.10; these are empty lone pairs and empty antibonding orbitals. The set of found core orbitals, lone pairs and NBOs is the *natural Lewis structure* of the molecule.

To estimate the deviation from this Lewis model (that is, the delocalization effects), a second-order perturbative analysis of the Fock matrix is done: this matrix is built in the NBO basis and, for each term, the quantity:

$$\Delta E_{\sigma\sigma^*}^{(2)} = -2\frac{\left\langle \sigma \left| \hat{F} \right| \sigma^* \right\rangle}{\epsilon_{\sigma^*} - \epsilon_\sigma}$$

is calculated, where σ and σ^* are an occupied and an empty NBO, respectively, and ϵ_σ and ϵ_{σ^*} are their corresponding eigenvalues (with respect to the Fock matrix). This quantity is interpreted as the stabilization of the molecule achieved by delocalizing the electrons in σ into σ^*.

The NBO analysis provides information that can complement that obtained with the AIM theory, such as the degree of delocalization of the electron density or the nature of the bonds (whether they are short-range, strong covalent bonds or long range, weak non-covalent ones).

Chapter 3

Results and Discussion

The general purposes of this work were to establish a systematic way of studying metal-α-synuclein interaction sites, to validate it by comparing the results it provides with experimental results for Cu^{2+} reported in the literature and to apply it to study other sites and other metal cations. This systematic way involves building coordination complexes between a metal cation and a dipeptide cut from α-synuclein's amino acid sequence, optimizing their geometries and computing a Gibbs free energy for them in the way described in the previous chapter. Each one of these built coordination complexes is intended to represent a binding site.

Table 3.1 lists the binding sites addressed in the present study, which are divided into two groups: the experimentally characterized sites for Cu^{2+} (shown in blue) and the ones that are proposed in this work since their structures could, in principle, be similar (shown in orange). The *Name* column contains the names used to refer to each site in the rest of the tables in this chapter. In the text, the sites are referred to by their numbers in this table. Figure 3.1 displays the location of each studied site in α-synuclein's primary structure, together with the full chemical formulas of some of them. Figure 3.2 shows the location of those sites in the secondary structure. In these figures, the experimental and additional proposed complexes are also shown in

Table 3.1: List of complexes studied, each one with Cu^{2+}, Zn^{2+} and Al^{3+}. The horizontal lines mark the limits of the three α-synuclein domains. The experimentally characterized Cu^{2+} binding sites mentioned in the literature are presented in blue, while the additional ones proposed in this work are presented in orange. No. = site number. α-syn seq. = position in α-synuclein sequence. R_1 res. = residue bearing R_1. L_1 res. = residue bearing L_1. The *Name* column, as can be seen, just consists of the four previous ones separated by dots, and will be used in the rest of the tables to refer to each site.

No.	α-syn seq.	R_1 res.	L_1 res.	L_2	Name
1	1-2	Met	Asp	H_2O	1-2.Met.Asp.H_2O
2	1-2	NacMet	Asp	H_2O	1-2.NacMet.Asp.H_2O
3	1-2-50	Met	Asp	Hid	1-2-50.Met.Asp.Hid
4	1-2-50	NacMet	Asp	Hid	1-2-50.NacMet.Asp.Hid
5	1-2-50	Met	Asp	Hie	1-2-50.Met.Asp.Hie
6	1-2-50	NacMet	Asp	Hie	1-2-50.NacMet.Asp.Hie
7	8-9	Leu	Ser	H_2O	8-9.Leu.Ser.H_2O
8	41-42	Gly	Ser	H_2O	41-42.Gly.Ser.H_2O
9	43-44	Lys	Thr	H_2O	43-44.Lys.Thr.H_2O
10	49-50	Val	Hie	H_2O	49-50.Val.Hie.H_2O
11	53-54	Ala	Thr	H_2O	53-54.Ala.Thr.H_2O
12	74-75	Val	Thr	H_2O	74-75.Val.Thr.H_2O
13	97-98	Lys	Asp	H_2O	97-98.Lys.Asp.H_2O
14	114-115	Glu	Asp	H_2O	114-115.Glu.Asp.H_2O
15	118-119	Val	Asp	H_2O	118-119.Val.Asp.H_2O
16	121-122	Asp	Asn	H_2O	121-122.Asp.Asn.H_2O
17	134-135	Gln	Asp	H_2O	134-135.Gln.Asp.H_2O
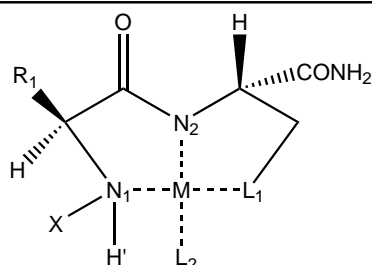
blue and orange, respectively. This color code is subsequently used through this chapter. Each one of these binding sites was studied with Cu^{2+}, Zn^{2+} and Al^{3+}, with both the M06 and the ωB97X-D functionals.

The purpose of including the experimentally found Cu^{2+} complexes in this computational study was to validate the methodology used here by comparing the theoretical geometries with the experimentally determined ones and also by checking whether the lowest predicted Gibbs free energies corresponded to the experimentally found complexes.

The purposes of studying additional sites and addressing also Zn^{2+} and Al^{3+} complexes were to determine if any site not found experimentally is also thermodynamically feasible, and to find whether Zn^{2+} and Al^{3+} complexes follow trends analogous to Cu^{2+} ones, both structurally and energetically.

The DFT geometry optimizations (with both the M06 and the ωB97X-D functionals) of all three series of metal complexes with dipeptide models converged to true minima.

Visualization of the optimized structure of complex **1**, which corresponds to the highest-affinity Cu^{2+} binding site according to experiment, revealed, for both the M06 and the ωB97X-D functionals, a nearly square planar (D_{4h}) disposition of the coordinating atoms (see figure 3.3), in agreement with the predictions made by electron paramagnetic resonance (EPR), electronic spectroscopy studies and QM/MM molecular dynamics simulations [152]. The three complexes involving Hid/Hie 50 and proposed by De Ricco [144] to exist at high pH and high Cu^{2+} concentrations (**3**, **5** and **10**, with both functionals) were also minimized to a distorted square planar geometry (see figure 3.4). Complexes **3** and **5** only differed by the nitrogen atom in the imidazole ring of histidine binding Cu^{2+} (the ε nitrogen in **3** and the δ one in **5**), while **10** involved the backbone amide nitrogen atoms of Val 49 and Hie 50, the δ nitrogen of Hie 50 and a water molecule.

Regarding the main low affinity Cu^{2+} site at the C-terminus identified
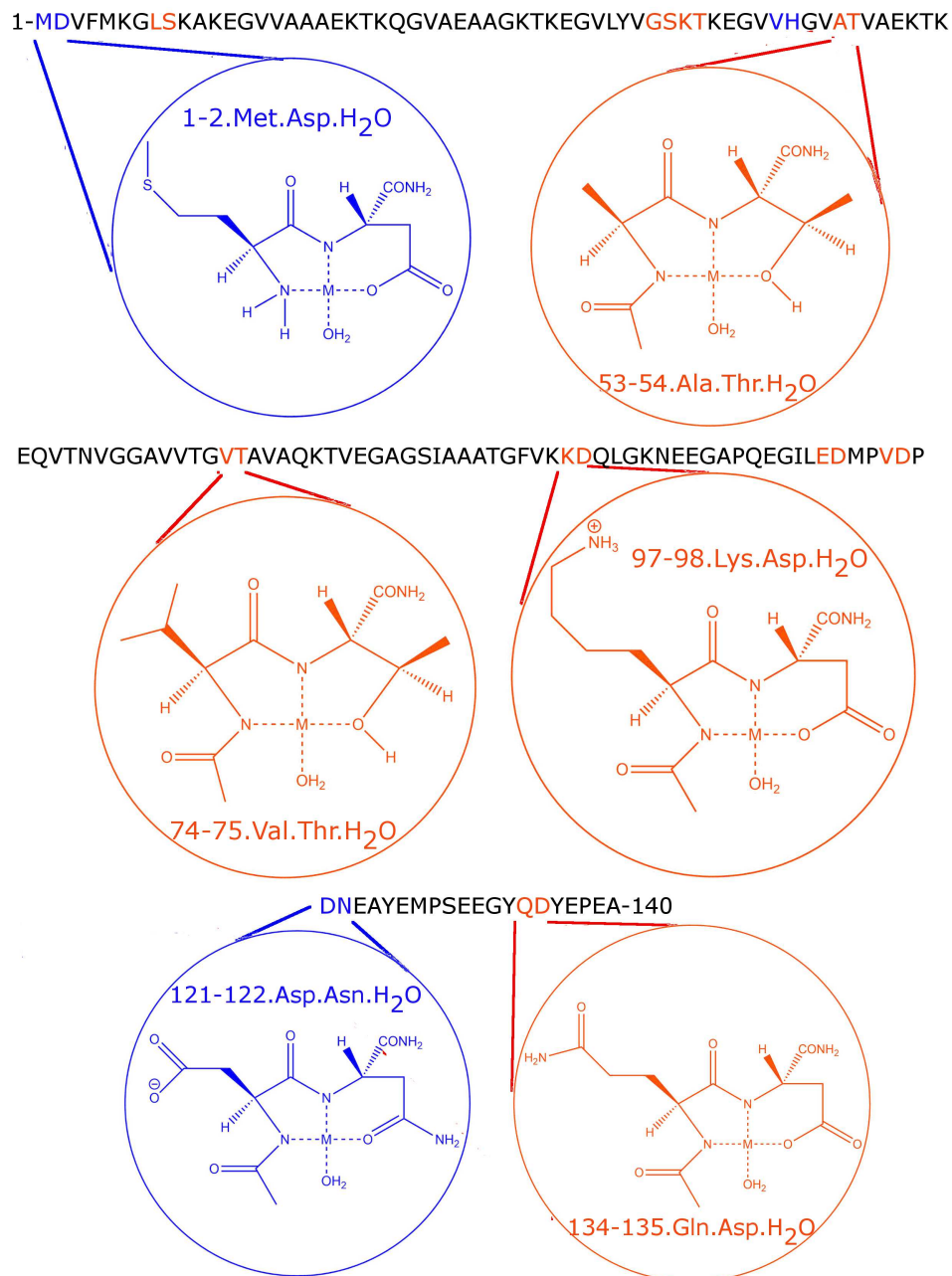
Figure 3.1: Graphical representation of α-synuclein's primary structure, showing the location of both the experimentally proposed Cu^{2+} sites (in blue) and the additional ones proposed in this study (in orange), as well as diagrams of some selected sites.
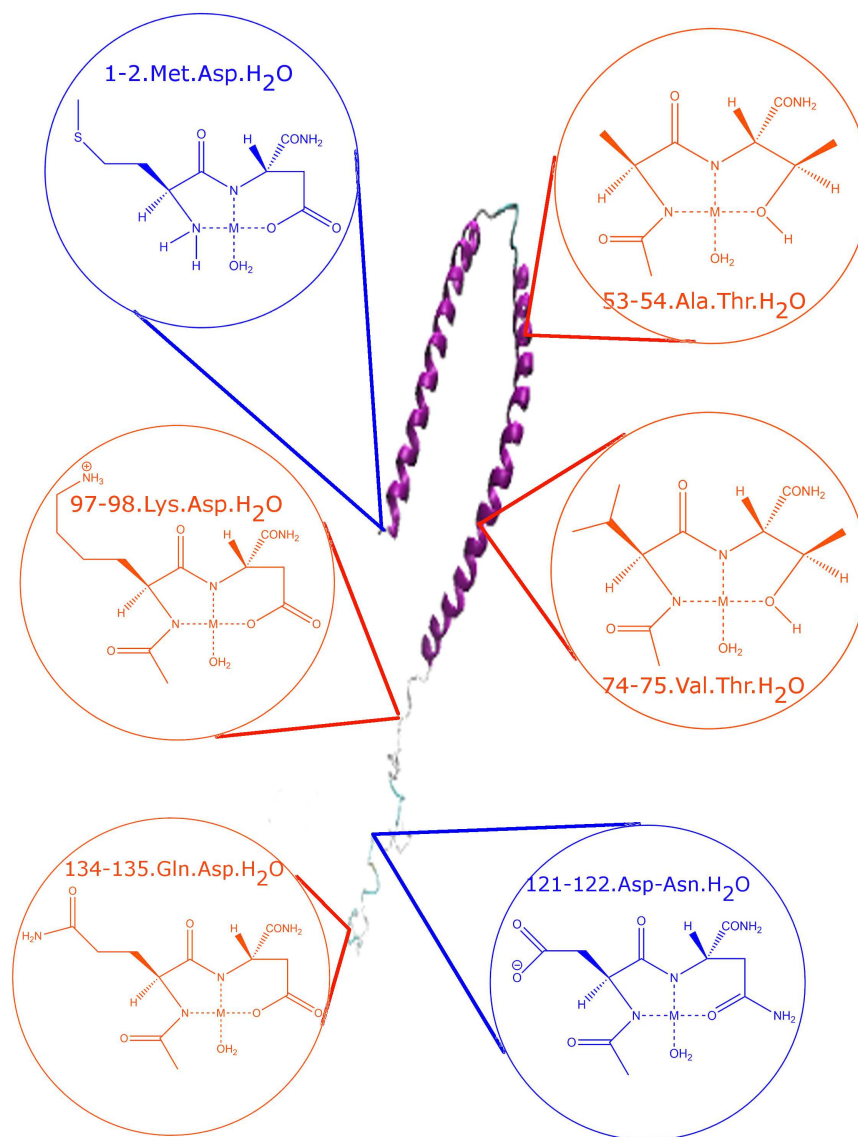
Figure 3.2: Graphical representation of α-synuclein's secondary structure, showing the location of both the experimentally proposed Cu^{2+} sites (in blue) and the additional ones proposed in this study (in orange), as well as diagrams of some selected sites.
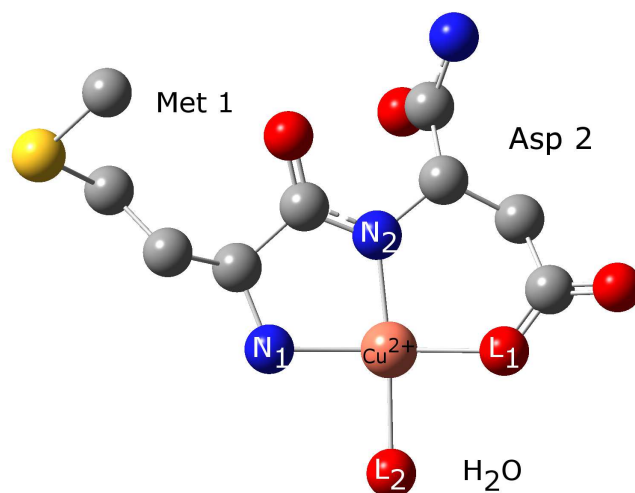
Figure 3.3: Optimized structure (UM06/6-311+G(d,p)/SMD) of **1**, the model representing the first experimentally determined high-affinity copper binding site in α-synuclein. The structure obtained with ωB97X-D is similar. Hydrogen atoms have been omitted for clarity.
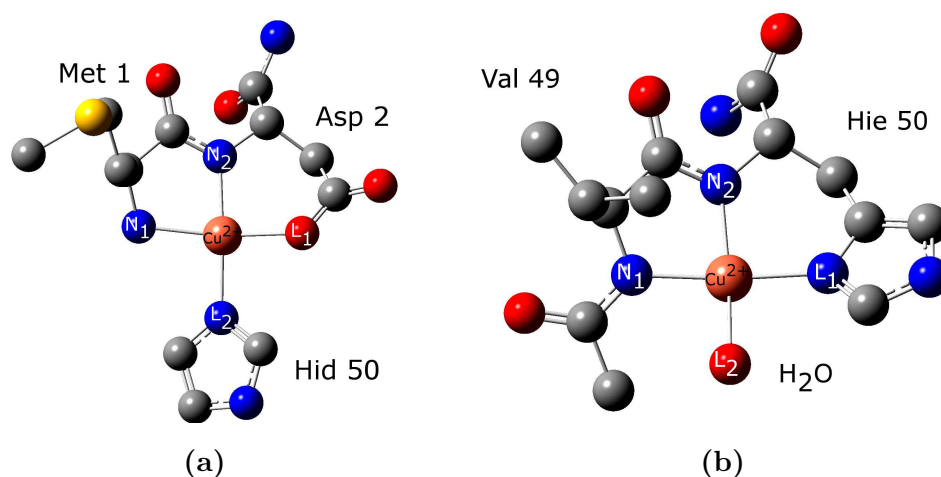
Figure 3.4: Two (**3**, a, and **10**, b) of the three (**3**, **5** and **10**) optimized structures (UM06/6-311+G(d,p)/SMD) representing the experimentally determined high-affinity copper binding site involving Hid/Hie 50. The complex with Hie (**5**) is similar to the one with Hid (**3**). The corresponding ones obtained with ωB97X-D are similar. Hydrogen atoms and part of the Hid residue have been omitted for clarity.
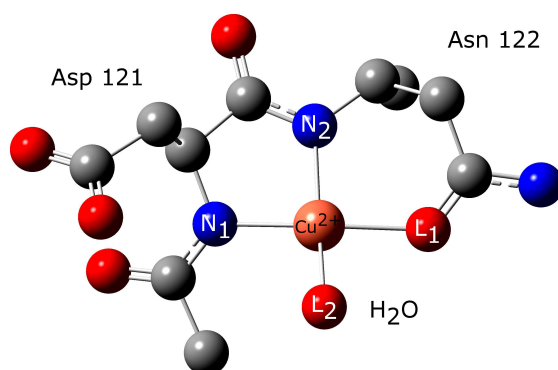
Figure 3.5: Optimized structure (UM06/6-311+G(d,p)/SMD) of **16**, which represents the experimentally determined low-affinity copper binding site in α-synuclein. The structure obtained with ωB97X-D is similar. Hydrogen atoms and the backbone carbonyl oxygen of Asn 122 have been omitted for clarity.

by means of spectroscopic techniques and centered on Asp 121 [142], minimization of complex **16** led (with both functionals) to a nearly square planar structure where the Cu^{2+} cation was bound to the carbonyl oxygen in the side chain of Asn 122, and where the backbone nitrogen atoms of Asp 121 and Asn 122 and a water molecule completed the coordination sphere (see figure 3.5).

In the following sections, the similarities and differences among all the studied sites, metal cations and density functionals will be analyzed and commented on.

3.1 Geometries

In this section, the nomenclature used to refer to the four atoms coordinating the metal will be the one in the complexes' general scheme (N_1, N_2, L_1, L_2), which is reproduced below.
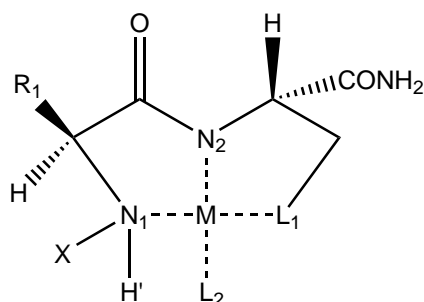
In the case of Cu^{2+} complexes, all of them show the previously mentioned distorted square planar geometry, with only minor differences among sites and with only slight deviations from a perfectly planar structure. This is suggested by the values of the N_1-N_2-M-L_1 and the N_2-N_1-M-L_2 dihedrals, which can be used as a measure of the complexes' planarity, since the first one is related to the deviation of L_1 from the plane determined by the metal and the two backbone nitrogen atoms (N_1 and N_2) and the second one measures the separation of L_2 from that same plane (the higher their difference with $\pm 180°$, the lower the planarity of the complexes). N_1-N_2-Cu^{2+}-L_1 oscillates between -161.4° and 167.7° in the M06 series and between -163.0° and 169.5° in the ωB97X-D series. N_2-N_1-Cu^{2+}-L_2 ranges between -163.8° and 155.3° in the M06 series, while varying between -172.7° and 159.4° in the ωB97X-D one. In these dihedral angle values, the negative signs indicate that the L_1 ligand is "above" the plane, while the positive signs mean that it lies "below" it, whereas for the L_2 ligand it is the other way. Therefore, in absolute terms, both functionals predict that the L_1 and L_2 ligands will not deviate more than 25° from the N_1-Cu^{2+}-N_2 plane.

The N_1-Cu^{2+}-N_2, N_2-Cu^{2+}-L_1, L_1-Cu^{2+}-L_2 and L_2-Cu^{2+}-N_1 angles, whose proximity to 90° indicates how tetragonal the complexes are, vary between 80.1° and 108.6° in the M06 series, whereas in the ωB97X-D series, they oscillate between 79.7° and 108.6°. In most of the complexes, especially if the amino acid residue carrying L_1 is a Ser or a Thr, the N_2-Cu^{2+}-L_1 and the N_1-Cu^{2+}-L_2 angles are the ones lying the farthest from 90° (N_2-Cu^{2+}-L_1 is always around 80° while N_1-Cu^{2+}-L_2 is often over 100°). This fact could be

60

explained by the repulsion between the electrons of Cu^{2+} and the lone pair on the hydroxyl oxygen of Ser and Thr being greater than their electrostatic attraction and by the repulsion between the acetyl group in N_1 and H_2O.

Bond lengths between Cu^{2+} and the four atoms surrounding it (collected in table 3.2) take values in the 1.92-2.18 Å interval. The Cu^{2+}-L_2 distances are greater than 2 Å in all cases (both with water and with a nitrogen atom of an imidazole ring), suggesting that the L_2 ligand is more labile than the other three. On the other hand, the Cu^{2+}-N_2 distances are always less than or equal to 2 Å and also the Cu^{2+}-N_1 ones (except for complexes **1**, **3** and **5**, with both functionals). These exceptions are precisely the complexes in which N_1 is not acetylated and is therefore not negatively charged, which suggests the idea that the deprotonated backbone nitrogen atoms, with a negative formal charge, interact more strongly with the cation, in comparison with the terminal nitrogen atom (see figure 3.6). Also, whenever L_1 is either Ser or Thr, the Cu^{2+}-L_1 distance is above 2.13 Å, suggesting a comparatively weaker interaction between each of these two residues and Cu^{2+}. When L_1 is Asp or Hie, this distance stays around 2 Å.
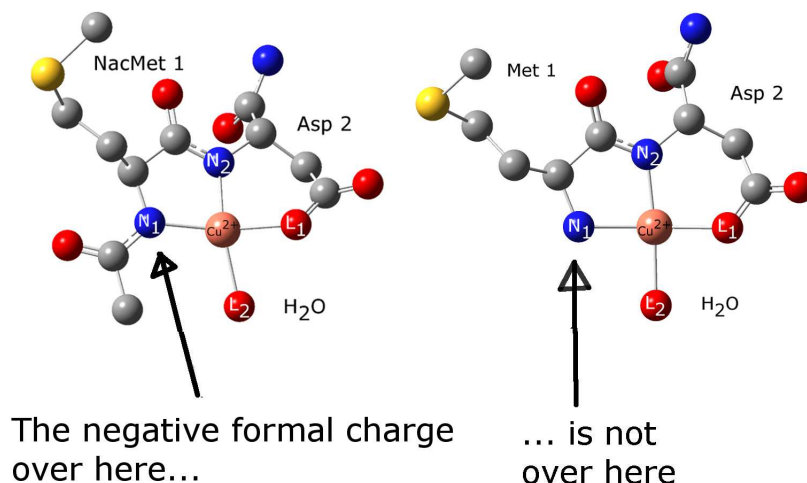

Figure 3.6: Representation of complexes **2** (left) and **1** (right), pointing out the extra negative formal charge of **2**, leading to the lower M-N_1 distances. The same situation occurs for sites **3** and **4**, and for **5** and **6**. Hydrogen atoms have been omitted for clarity.

Table 3.2: Distances between Cu^{2+} and the atoms surrounding it in each studied complex. In each entry, the values for the M06 (left) and ωB97X-D (right) functionals are separated by a slash. Values in Å.

No.	Name	Cu^{2+}-N_1 M06/ωB97X-D	Cu^{2+}-N_2 M06/ωB97X-D	Cu^{2+}-L_1 M06/ωB97X-D	Cu^{2+}-L_2 M06/ωB97X-D
1	1-2.Met.Asp.H$_2$O	2.01/2.02	1.93/1.94	1.96/1.97	2.07/2.07
2	1-2-NacMet.Asp.H$_2$O	1.97/1.98	1.94/1.95	1.99/1.99	2.10/2.12
3	1-2-50.Met.Asp.Hid	2.04/2.05	1.95/1.96	1.99/1.99	2.00/2.00
4	1-2-50.NacMet.Asp.Hid	1.98/1.99	1.96/1.96	2.00/2.02	2.02/2.01
5	1-2-50.Met.Asp.Hie	2.05/2.06	1.96/1.96	1.99/1.99	2.02/2.02
6	1-2-50.NacMet.Asp.Hie	1.99/2.01	1.96/1.97	2.03/2.03	2.02/2.02
7	8-9.Leu.Ser.H$_2$O	1.96/1.97	1.92/1.92	2.17/2.18	2.04/2.04
8	41-42.Gly.Ser.H$_2$O	1.96/1.97	1.93/1.94	2.15/2.16	2.05/2.06
9	43-44.Lys.Thr.H$_2$O	1.97/1.98	1.92/1.93	2.15/2.14	2.05/2.04
10	49-50.Val.Hie.H$_2$O	1.95/1.96	1.99/1.98	1.98/1.99	2.18/2.12
11	53-54.Ala.Thr.H$_2$O	1.96/1.98	1.93/1.93	2.14/2.14	2.04/2.07
12	74-75.Val.Thr.H$_2$O	1.96/1.97	1.92/1.93	2.13/2.14	2.05/2.05
13	97-98.Lys.Asp.H$_2$O	1.97/1.98	1.95/1.95	1.97/1.98	2.09/2.08
14	114-115.Glu.Asp.H$_2$O	1.97/1.98	1.95/1.95	1.99/1.99	2.09/2.09
15	118-119.Val.Asp.H$_2$O	1.95/1.96	1.95/1.96	1.97/1.98	2.12/2.12
16	121-122.Asp.Asn.H$_2$O	1.95/1.97	1.95/1.95	2.01/2.01	2.09/2.08
17	134-135.Gln.Asp.H$_2$O	1.97/1.98	1.95/1.95	1.98/1.99	2.08/2.09

The Zn^{2+} complexes whose L_1 residue is Asp, Asn, Hid or Hie are tetracoordinated and their geometries are at some point between a square planar and a tetrahedral one (see figure 3.7). The N_1-N_2-Zn^{2+}-L_1 and N_2-N_1-Zn^{2+}-L_2 dihedrals would equal $\pm 120°$ in a regular tetrahedron. Considering only those complexes, the N_1-N_2-Zn^{2+}-L_1 dihedral falls between -136.8° and 155.8° in the M06 series and between -135.5° and 154.0° in the ωB97X-D series. The N_2-N_1-Zn^{2+}-L_2 dihedral is between -124.0° and 142.8° in the M06 series, while in the ωB97X-D one, it lies between -119.3° and 143.0°. The signs criterion is the same as for the Cu^{2+} complexes. The tetracoordinated Zn^{2+} complexes, therefore, differ from an ideal square planar structure considerably more than Cu^{2+} complexes do, reaching as much as 44.5° (in the case of L_1) or 60.7° (in the case of L_2).

The N_1-Zn^{2+}-N_2, N_2-Zn^{2+}-L_1, L_1-Zn^{2+}-L_2 and L_2-Zn^{2+}-N_1 angles, in this subset of complexes, are quite similar to the corresponding Cu^{2+} ones, the
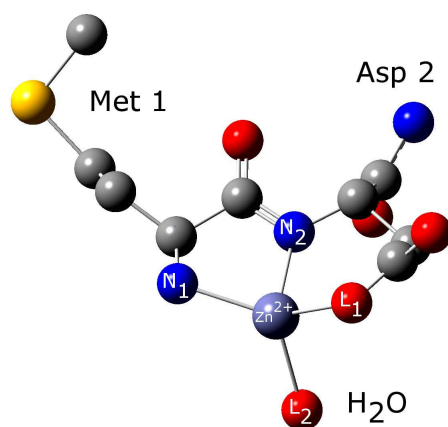
Figure 3.7: Optimized structure (UM06/6-311+G(d,p)/SMD) of **1** with Zn^{2+}. Hydrogen atoms have been omitted for clarity. Note the more tetrahedral shape of this complex in comparison with the analogous Cu^{2+} one.

most remarkable differences being in the L_2-Zn^{2+}-N_1 angles, which differ noticeably more from 90° than their counterparts in the Cu^{2+} set.

The distances between Zn^{2+} and N_1, N_2, L_1 or L_2, again in this subset, are slightly higher than those of the corresponding Cu^{2+} complexes in all cases. These distances are presented in table 3.3. Given that Zn^{2+} and Cu^{2+} have similar ionic radii, these differences could be explained by Zn^{2+} bonds being weaker than Cu^{2+} bonds.

On the contrary, Zn^{2+} complexes with Ser or Thr as L_1 are tricoordinated (see figure 3.8). In these cases, L_1 is totally out of the coordination sphere, with Zn^{2+}-L_1 distances of up to 3.5 Å (for complex **7** with ωB97X-D), the lowest one being 2.98 Å (for complex **11** with M06). This suggests that the earlier mentioned repulsion between Cu^{2+} and L_1 is even stronger with Zn^{2+}. What is more, by visual inspection of these Zn^{2+} complexes, a hydrogen bond could exist between L_2 (H_2O) and L_1 (Ser or Thr).

The N_2-N_1-Zn^{2+}-L_2 dihedral in this set oscillates between -169.1° and 166.4° in the M06 series and between -173.1° and 154.9° in the ωB97X-D series, so the H_2O molecule is never farther than 25.1° away from the N_1-

Table 3.3: Distances between Zn^{2+} and each surrounding atom in each studied tetracoordinated Zn^{2+} complex. In each entry, the values for the M06 (left) and ωB97X-D (right) functionals are separated by a slash. Values in Å.

No.	Name	Zn^{2+}-N_1 M06/ωB97X-D	Zn^{2+}-N_2 M06/ωB97X-D	Zn^{2+}-L_1 M06/ωB97X-D	Zn^{2+}-L_2 M06/ωB97X-D
1	1-2.Met.Asp.H_2O	2.09/2.10	2.00/2.01	2.04/2.04	2.09/2.10
2	1-2-NacMet.Asp.H_2O	2.00/2.01	2.01/2.04	2.04/2.05	2.15/2.13
3	1-2-50.Met.Asp.Hid	2.17/2.16	1.99/2.01	2.12/2.07	2.02/2.03
4	1-2-50.NacMet.Asp.Hid	2.04/2.03	2.01/2.03	2.09/2.08	2.04/2.06
5	1-2-50.Met.Asp.Hie	2.23/2.24	2.02/2.04	2.14/2.14	2.07/2.06
6	1-2-50.NacMet.Asp.Hie	2.07/2.08	2.05/2.06	2.18/2.21	2.08/2.07
10	49-50.Val.Hie.H_2O	1.99/2.01	2.06/2.06	2.04/2.05	2.33/2.33
13	97-98.Lys.Asp.H_2O	2.03/2.04	2.06/2.06	2.07/2.07	2.20/2.22
14	114-115.Glu.Asp.H_2O	2.02/2.03	2.04/2.05	2.09/2.08	2.20/2.24
15	118-119.Val.Asp.H_2O	2.03/2.04	2.04/2.04	2.08/2.08	2.21/2.22
16	121-122.Asp.Asn.H_2O	2.00/2.02	2.02/2.03	2.11/2.11	2.12/2.13
17	134-135.Gln.Asp.H_2O	2.03/2.05	2.06/2.05	2.08/2.07	2.22/2.24

Zn^{2+}-N_2 plane. The N_1-Zn^{2+}-N_2 angle ranges from 84.2° to 85.6° in the M06 series and from 84.6° to 85.1° in the ωB97X-D series, the N_2-Zn^{2+}-L_1 angle varies from 122.8° to 138.7° in the M06 series and from 120.9° to 142.2° in the ωB97X-D series and the N_1-Zn^{2+}-L_2 angle is between 135.9° and 152.0° in the M06 series and from 132.6° and 151.4° in the ωB97X-D series. Together, these results show that these complexes are nearly trigonal planar, with one of the three angles (N_1-Zn^{2+}-N_2) being close to 90° and the other two around 135°. In other words, the water molecule is lying on the N_1-Zn^{2+}-N_2 angle bisector (with C_{2v} symmetry).

The distances from these three ligands to the Zn^{2+} cation (collected in table 3.4) are not particularly different from the corresponding ones in the Cu^{2+} complexes, but the Zn^{2+}-L_2 distances (in this subset, L_2 is always water), unlike in the tetracoordinated complexes, are consistently slightly smaller than in the Cu^{2+} series, which could be due to water interacting better with Zn^{2+} when L_1 is outside the coordination sphere.
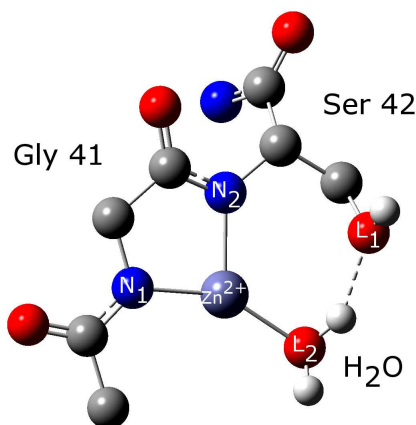
Figure 3.8: Optimized structure (UM06/6-311+G(d,p)/SMD) of **8** with Zn^{2+}. Hydrogen atoms (except the ones of the water molecule and of the Ser hydroxyl group) have been omitted for clarity. The ωB97X-D structure is qualitatively similar. Note the trigonal shape of this complex (shared by all the others with Ser or Thr as L_1) and the apparent hydrogen bond interaction indicated by the dotted line.

Table 3.4: Distances between Zn^{2+} and the three surrounding atoms in each studied tricoordinated Zn^{2+} complex. In each entry, the values for the M06 (left) and ωB97X-D (right) functionals are separated by a slash. Values in Å.

No.	Name	Zn^{2+}-N_1	Zn^{2+}-N_2	Zn^{2+}-L_2
		M06/ωB97X-D	M06/ωB97X-D	M06/ωB97X-D
7	8-9.Leu.Ser.H$_2$O	1.96/2.00	1.99/1.98	2.01/2.02
8	41-42.Gly.Ser.H$_2$O	1.97/1.98	2.01/2.03	1.99/2.01
9	43-44.Lys.Thr.H$_2$O	1.97/2.00	2.01/1.99	1.99/2.02
11	53-54.Ala.Thr.H$_2$O	1.96/1.99	1.98/1.98	1.99/2.02
12	74-75.Val.Thr.H$_2$O	1.97/1.98	1.99/1.98	1.99/2.01

All Al^{3+} complexes display a distorted tetrahedral geometry (see figure 3.9). The N_1-N_2−Al^{3+}-L_1 dihedral in complex **5** with M06 (which has a value of -164.3°) is the closest one to ±180°. This dihedral ranges from -132.6° to 131.0° in the M06 set and from -129.0° to 125.4° in the ωB97X-D one. As for the N_2-N_1−Al^{3+}-L_2 dihedrals, they lie even farther from ±180°; the closest one (in complex **12** with ωB97X-D) is 142.0°. These take values between -118.9° and 111.7° in the M06 series, whereas, in the ωB97X-D series, their values are between -123.5° and 121.7°.
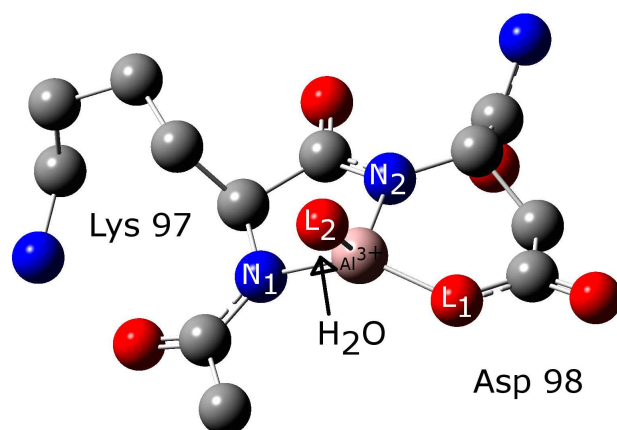
Figure 3.9: Optimized structure (UM06/6-311+G(d,p)/SMD) of **13** with Al^{3+}. Hydrogen atoms have been omitted for clarity. The ωB97X-D structure is qualitatively similar. Note the tetrahedral shape of this complex, shared by all the other Al^{3+} ones.

Distances between Al^{3+} and N_1, N_2, L_1 or L_2 (presented in table 3.5) are systematically lower than in Cu^{2+} and Zn^{2+}, which is attributable to the smaller ionic radius of Al^{3+} compared to the ones of Cu^{2+} or Zn^{2+}.

Table 3.5: Distances between Al^{3+} and the four surrounding atoms in each studied Al^{3+} complex. In each entry, the values for the M06 (left) and ωB97X-D (right) functionals are separated by a slash. Values in Å.

No.	Name	Al^{3+}-N_1 M06/ωB97X-D	Al^{3+}-N_2 M06/ωB97X-D	Al^{3+}-L_1 M06/ωB97X-D	Al^{3+}-L_2 M06/ωB97X-D
1	1-2.Met.Asp.H_2O	1.92/1.92	1.82/1.82	1.75/1.76	1.81/1.82
2	1-2-NacMet.Asp.H_2O	1.83/1.83	1.83/1.83	1.77/1.78	1.83/1.84
3	1-2-50.Met.Asp.Hid	1.93/1.94	1.82/1.83	1.77/1.78	1.88/1.88
4	1-2-50.NacMet.Asp.Hid	1.84/1.85	1.83/1.84	1.78/1.79	1.89/1.89
5	1-2-50.Met.Asp.Hie	1.93/1.93	1.82/1.83	1.77/1.78	1.88/1.89
6	1-2-50.NacMet.Asp.Hie	1.84/1.84	1.83/1.84	1.77/1.79	1.91/1.89
7	8-9.Leu.Ser.H_2O	1.82/1.83	1.83/1.82	1.86/1.87	1.81/1.82
8	41-42.Gly.Ser.H_2O	1.83/1.83	1.82/1.82	1.85/1.87	1.82/1.82
9	43-44.Lys.Thr.H_2O	1.83/1.83	1.82/1.82	1.84/1.84	1.82/1.83
10	49-50.Val.Hie.H_2O	1.82/1.83	1.83/1.83	1.88/1.88	1.83/1.83
11	53-54.Ala.Thr.H_2O	1.82/1.83	1.82/1.82	1.84/1.84	1.82/1.83
12	74-75.Val.Thr.H_2O	1.82/1.83	1.82/1.82	1.84/1.84	1.82/1.83
13	97-98.Lys.Asp.H_2O	1.83/1.84	1.83/1.83	1.76/1.76	1.84/1.85
14	114-115.Glu.Asp.H_2O	1.83/1.83	1.84/1.84	1.76/1.76	1.84/1.85
15	118-119.Val.Asp.H_2O	1.83/1.83	1.84/1.84	1.76/1.77	1.84/1.83
16	121-122.Asp.Asn.H_2O	1.82/1.83	1.83/1.84	1.79/1.80	1.83/1.84
17	134-135.Gln.Asp.H_2O	1.83/1.84	1.83/1.83	1.76/1.76	1.84/1.85

3.2 Energies

Table 3.6 reports the Gibbs free energies calculated for each studied complex. In this table, the data corresponding to the five complexes with the most negative energies for each metal and for each functional are emphasized.

Among Cu^{2+} complexes, the five most stable ones are, from the lowest to the highest, **6** (-87.5 kcal/mol), **15** (-84.5 kcal/mol), **4** (-83.9 kcal/mol), **10** (-83.8 kcal/mol) and **14** (-83.7 kcal/mol) for M06 and **6** (-90.0 kcal/mol), **15** (-85.8 kcal/mol), **4** (-85.4 kcal/mol), **10** (-83.5 kcal/mol) and **16** (-83.3 kcal/mol) for ωB97X-D. As can be seen, three experimentally proposed complexes (**6**, **4** and **10**) are among the five most stable ones in the M06 series, while for ωB97X-D, there are four (**6**, **4**, **10** and **16**). This, together with the fact that the theoretically predicted geometries of Cu^{2+} complexes agree with the experimentally proposed ones, suggests that the methodology used

here, despite its simplicity, can yield meaningful results and can therefore be applied to study new binding sites and metals.

This being said, it is remarkable that Cu^{2+} complexes **15** and **14** (involving Val 118-Asp 119 and Glu 114-Asp 115, respectively), although not experimentally characterized, are also thermodynamically stable according to this study (the second and the fifth most stable ones, with -84.5 kcal/mol for **15** and -83.7 kcal/mol for **14** with M06, and the second and the sixth most stable ones, with -85.8 kcal/mol for **15** and -81.7 kcal/mol for **14** with ωB97X-D).

Table 3.6: Gibbs free energies associated to each metal-dipeptide complex, calculated as the free energy changes of the working reaction given in the *Methodology* chapter. In each entry, the values for the M06 (left) and ωB97X-D (right) functionals are separated by a slash. Values in kcal/mol.

No.	Name	Cu^{2+} M06/ωB97X-D	Zn^{2+} M06/ωB97X-D	Al^{3+} M06/ωB97X-D
1	1-2.Met.Asp.H$_2$O	-68.2/-69.8	-50.1/-55.1	-40.7/-45.0
2	1-2-NacMet.Asp.H$_2$O	-76.8/-78.0	-62.8/-65.2	**-66.5**/ **-69.0**
3	1-2-50.Met.Asp.Hid	-75.6/-78.5	-53.7/-59.2	-51.3/-57.9
4	1-2-50.NacMet.Asp.Hid	**-83.9/-85.4**	**-65.8/-68.8**	**-77.6/-83.7**
5	1-2-50.Met.Asp.Hie	-75.2/-80.3	-53.2/-61.9	-53.2/-60.1
6	1-2-50.NacMet.Asp.Hie	**-87.5/-90.0**	**-63.3/-68.7**	**-74.4/-84.9**
7	8-9.Leu.Ser.H$_2$O	-69.0/-70.7	-56.2/-60.1	-35.5/-39.0
8	41-42.Gly.Ser.H$_2$O	-72.3/-74.3	-59.4/-64.8	-34.7/-38.8
9	43-44.Lys.Thr.H$_2$O	-71.5/-74.6	-56.8/-62.8	-34.8/-40.3
10	49-50.Val.Hie.H$_2$O	**-83.8/-83.5**	-62.5/**-66.3**	-63.1/-64.9
11	53-54.Ala.Thr.H$_2$O	-75.2/-77.4	-60.3/-63.9	-39.4/-43.6
12	74-75.Val.Thr.H$_2$O	-77.6/-79.1	-62.0/-66.2	-42.1/-46.7
13	97-98.Lys.Asp.H$_2$O	-76.3/-77.4	-57.4/-59.5	-58.9/-61.8
14	114-115.Glu.Asp.H$_2$O	**-83.7**/-81.7	**-63.3**/-64.5	**-68.3/-68.4**
15	118-119.Val.Asp.H$_2$O	**-84.5/-85.8**	**-64.6/-69.1**	**-67.3/-74.6**
16	121-122.Asp.Asn.H$_2$O	-81.9/**-83.3**	**-63.8/-66.7**	-58.5/-63.6
17	134-135.Gln.Asp.H$_2$O	-77.8/-80.2	-59.1/-63.0	-62.7/-65.3

Comparison of complexes **1**, **3** and **5** reveals that Cu^{2+} complexes with Hid or Hie as the fourth ligand (**3** and **5**) have lower energies than Cu^{2+} complexes with water at this same position (**1**). As a matter of fact, the M06 energies of **1**, **3** and **5** are -68.2, -75.6 and -75.2 kcal/mol, respectively, while the ωB97X-D ones are -69.8, -78.5 and -80.3 kcal/mol, respectively). This is also in agreement with the experimental studies concluding that the 1-2-50 complexes (**3** and **5**) are favored over the 1-2 one (**1**) at high pH, when the nitrogen atoms in the histidine residue are deprotonated and, therefore, available to coordinate Cu^{2+}.

An interesting fact about the **1**-**6** group is the stabilization of Cu^{2+} complexes **1**, **3** and **5** when adding an acetyl group to the Met nitrogen (yielding complexes **2**, **4** and **6**, respectively). This is actually attributed to the stabilizing electrostatic interaction between Cu^{2+} and the already mentioned negative formal charge on the Met nitrogen (present in the acetylated complexes, **2**, **4** and **6**, but absent in the non acetylated ones, **1**, **3** and **5**), and not to the acetyl group itself. This stabilization supports the idea of a stronger bond between the metal cation and the deprotonated backbone nitrogen atoms carrying a negative formal charge (with respect to the formally uncharged, terminal Met nitrogen), already suggested by the smaller bond distances.

On the other hand, the least stable Cu^{2+} complexes are, from the highest to the lowest energies, **1** (-68.2 kcal/mol), **7** (-69.0 kcal/mol), **9** (-71.5 kcal/mol), **8** (-72.3 kcal/mol) and **5**/**11** (-75.2 kcal/mol both) for M06 and **1** (-69.8 kcal/mol), **7** (-70.7 kcal/mol), **8** (-74.3 kcal/mol), **9** (-74.6 kcal/mol) and **11**/**13** (-77.4 kcal/mol both) for ωB97X-D. Both functionals predict complex **1** to be the least favored one, an observation which seemingly contradicts the experimental results, but which can again be attributed to the absence of a formal negative charge on the Met nitrogen in **1**. This same reasoning could explain the fact that complexes **3** and **5** (found experimentally) are not among the most stable ones. Regarding complexes **7**, **8** and **9**, the

fact that they are always among the least stable ones is attributable to their lower electrostatic and dispersion interactions, since their anchoring sites (L_1 residues) are small uncharged residues like Ser or Thr instead of charged ones like Asp or large ones like Hid, Hie or Asn. This idea is in agreement with the higher Cu^{2+}-Ser and Cu^{2+}-Thr distances (in relation to Cu^{2+}-Asp, Cu^{2+}-Hie and Cu^{2+}-Asn distances) discussed in the previous section.

These trends followed by Cu^{2+} complexes can be translated almost without changes to Zn^{2+} ones: the most stable Zn^{2+} complexes are, from the lowest to the highest energies, **4** (-65.8 kcal/mol), **15** (-64.6 kcal/mol), **16** (-63.8 kcal/mol), **6** (-63.3 kcal/mol) and **14** (-63.3 kcal/mol) for M06 and **15** (-69.1 kcal/mol), **4** (-68.8 kcal/mol), **6** (-68.7 kcal/mol), **16** (-66.7 kcal/mol) and **10** (-66.3 kcal/mol) for ωB97X-D, while the least stable ones are, from the highest to the lowest energies, **1** (-50.1 kcal/mol), **5** (-53.2 kcal/mol), **3** (-53.7 kcal/mol), **7** (-56.2 kcal/mol) and **9** (-56.8 kcal/mol) for M06 and **1** (-55.1 kcal/mol), **3** (-59.2 kcal/mol), **13** (-59.5 kcal/mol), **7** (-60.1 kcal/mol) and **9** (-62.8 kcal/mol) for ωB97X-D. So the most stable sites are again the ones involving Met 1, Asp 2 and Hie 50, the one with Val 49 and Hie 50 and the ones involving Glu 114 and Asp 115, Val 118 and Asp 119, and Asp 121 and Asn 122, and the least stable ones are those that contain Ser or Thr as anchoring site, as well as the ones without a formal negative charge on Met terminal nitrogen.

For Al^{3+}, on the other hand, the most stable sites are, from the lowest to the highest energies, **4** (-77.6 kcal/mol), **6** (-74.4 kcal/mol), **14** (-68.3 kcal/mol), **15** (-67.3 kcal/mol) and **2** (-66.5 kcal/mol) for M06 and **6** (-84.9 kcal/mol), **4** (-83.7 kcal/mol), **15** (-74.6 kcal/mol), **2** (-69.0 kcal/mol) and **14** (-68.4 kcal/mol) for ωB97X-D, while the least stable ones are, from the highest to the lowest energies, **8** (-34.7 kcal/mol), **9** (-34.8 kcal/mol), **7** (-35.5 kcal/mol), **11** (-39.4 kcal/mol) and **1** (-40.7 kcal/mol) for M06 and **8** (-38.8 kcal/mol), **7** (-39.0 kcal/mol), **9** (-40.3 kcal/mol), **11** (-43.6 kcal/mol) and **1** (-45.0 kcal/mol) for ωB97X-D. Therefore, for Al^{3+}, the Val 49-Hie 50

and Asp 121-Asn 122 sites would not be especially favored, but the NacMet 1-Asp 2-H_2O, NacMet 1-Asp 2-Hid/Hie, 114 Glu-115 Asp and Val 118-Asp 119 would.

When comparing the three metal cations with one another, one of the first facts that can be noted is the difference in the energies' magnitudes. Cu^{2+} complexes range from -68.2 (1) to -87.5 kcal/mol (6) for M06 and from -69.8 kcal/mol (1) to -90 kcal/mol (6) for ωB97X-D; Zn^{2+} complexes, from -50.1 (1) to -65.8 kcal/mol (4) for M06 and from -55.1 kcal/mol (1) to -69.1 kcal/mol (15) for ωB97X-D and Al^{3+} complexes, from -34.7 (8) to -77.6 kcal/mol (4) for M06 and from -38.8 kcal/mol (8) to -84.9 kcal/mol (6) for ωB97X-D. As can be seen, Cu^{2+} complexes present the narrowest energy ranges (19.3 and 20.2 kcal/mol for M06 and ωB97X-D, respectively), followed by Zn^{2+} complexes (15.7 and 14.0 kcal/mol for M06 and ωB97X-D, respectively) and finally by Al^{3+} complexes, whose energy ranges are much larger (42.9 and 46.1 kcal/mol for M06 and ωB97X-D, respectively). For all the studied sites, the energy associated to the Cu^{2+} complex is considerably below (more negative) the ones associated to both the Zn^{2+} and the Al^{3+} complexes. This supports the fact that Cu^{2+} complexes have been much more addressed than Zn^{2+} or Al^{3+} ones in experimental studies. However, the relative stabilities of Zn^{2+} and Al^{3+} complexes are site-dependent. Al^{3+} complexes have higher (less negative) associated energies than Zn^{2+} ones when the Met nitrogen is not acetylated and, therefore, without a negative formal charge (sites 1, 3 and 5) and especially when the anchoring site is Ser, Thr or Asn (formally uncharged residues). Al^{3+} complexes have more negative energies than the analogous Zn^{2+} ones when the Met nitrogen is acetylated (complexes 2, 4 and 6) as well as in complexes 13, 14, 15 and 17 (which are exactly the ones with the formally charged Asp as the anchoring site L_1). As for site 10, the Al^{3+} complex is more stable than the Zn^{2+} according to M06 (-63.1 versus -62.5 kcal/mol), but less stable according to ωB97X-D (-64.9 versus -66.3 kcal/mol). These comparisons of Zn^{2+} and Al^{3+} suggest a higher contribution of electrostatics in Al^{3+} interactions (relative

to Zn^{2+}), in agreement with its higher formal charge.

Another fact related to this higher formal charge of Al^{3+} is the difference between the free energies associated with complexes **1** and **2**, **3** and **4**, and **5** and **6** (remember that **1**, **3** and **5** do not have an acetyl group on the terminal Met nitrogen while **2**, **4** and **6** do have it). It can be seen that a decrease in energy occurs with the three metals upon acetylation, but with Al^{3+} its magnitude is much larger (between 6.9 and 12.3 kcal/mol for Cu^{2+}, between 6.8 and 12.7 kcal/mol for Zn^{2+} and between 21.2 and 26.3 kcal/mol for Al^{3+}). What is more, when the anchoring site is Ser or Thr (the small uncharged residues), the energy of the corresponding complex is generally higher (less negative) than when it is Asp (charged), Hie or Asn (larger than Ser or Thr). This happens with the three studied cations, but this difference is much more remarkable in the case of Al^{3+} complexes. Compare, for example, complexes **6** and **7** with M06, whose difference for Cu^{2+} is 18.5 kcal/mol, for Zn^{2+} it is 7.1 kcal/mol and for Al^{3+}, 38.9 kcal/mol.

Comparison of the M06 results with the ωB97X-D ones shows that the ωB97X-D energies tend to be slightly lower than the M06 ones, which could reveal a certain relevance of dispersion interactions between the cations and the dipeptides. Even though this pattern is common to the three metals, it can be observed that, in the case of Zn^{2+} and Al^{3+}, the difference between functionals is higher than in the Cu^{2+} case in a consistent manner: while in Cu^{2+} the largest difference is 5.1 kcal/mol (for site **5**), in Zn^{2+} it reaches 8.7 kcal/mol (also for site **5**) and in Al^{3+}, 10.1 kcal/mol (for site **6**), suggesting a higher importance of dispersion forces in Zn^{2+} and Al^{3+} complexes in comparison with Cu^{2+} ones. Also, there are two complexes in which this pattern fails: Cu^{2+} complexes **10** (-83.8 kcal/mol for M06 and -83.5 kcal/mol for ωB97X-D) and **14** (-83.7 kcal/mol for M06 and -81.7 kcal/mol for ωB97X-D), but these can be attributed to the optimizations having converged to slightly different conformers of the dipeptides with each functional.

3.3 AIM analysis

The diagram representing the general structure of all the studied complexes (whose nomenclature is again used in this section) is reproduced again below.
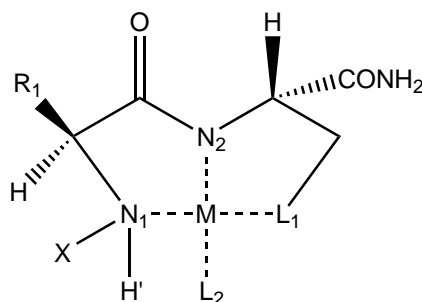
For tetracoordinated complexes, the topological analysis of the electron density found, in all sites and with the three metals, bond critical points on the straight lines connecting the cation and each one of the coordinating atoms. Apart from these, there are also ring critical points at the center of both the 5-membered and the 6-membered rings defined by the cation and N_1, N_2 and L_1 (numbers 5 and 6 in figure 3.10a), thus indicating how the complexes are also favored by the formation of these rings.

In tricoordinated Zn^{2+} complexes (**7**, **8**, **9**, **11** and **12**), the electron density presents bond critical points between Zn^{2+} and N_1, N_2 and L_2, but not between Zn^{2+} and L_1 (remember that L_1 is outside the coordination sphere in these cases). In these complexes, the presence of a bond critical point between water (L_2) and the oxygen atom on the side chain of L_1 (Ser or Thr) confirms the existence of a hydrogen bond, and there is also a ring critical point in this region, near the center of the 7-membered ring defined by the metal, the water molecule and L_1, up to N_2 (number 2 in figure 3.10b). This hydrogen bond could be another contribution to the more negative Gibbs free energies associated to these Zn^{2+} in comparison with the corresponding Al^{3+} ones; as an example, compare site number **7** with Zn^{2+} (-56.2 kcal/mol) and Al^{3+} (-35.5 kcal/mol), both with M06.

(a)   (b)
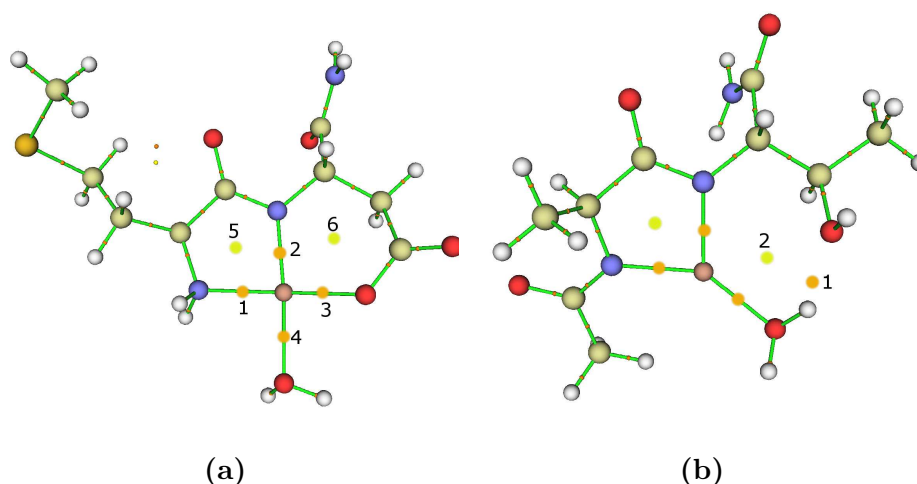
Figure 3.10: (a): Molecular graph of the Cu^{2+} complex at site **1**. Note the bond critical points 1-4 between Cu^{2+} and N_1, N_2, L_1 and L_2 and the ring critical points inside the 5 and 6-membered rings (5 and 6, respectively), which are common to all the studied complexes. (b): Molecular graph of the Zn^{2+} complex at site **11**, showing the bond critical point between one of the hydrogen atoms in the water molecule and the oxygen atom in the hydroxyl group of the Thr side chain and the ring critical point inside the 7-membered ring (1 and 2, respectively).

Figure 3.11 contains the contour maps of the Laplacian of the electron density ($\nabla^2\rho$) for site **16** with Cu^{2+}, Zn^{2+} and Al^{3+}, each one in two different planes. For the other sites, the plots are qualitatively similar. As can be observed, the regions with a negative value of $\nabla^2\rho$ (delimited by a thick line in figure 3.11) are always in the vicinity of N_1, N_2, L_1 and L_2 and they do not reach the internuclear region between them and the cation. This point is confirmed by the fact that $\nabla^2\rho$ is always positive at the corresponding bond critical points (as reported in table 3.7), which means that the electron density is locally depleted at these points. Therefore, the interactions between the cations and the dipeptides are non-covalent interactions.

Table 3.7 reports the electron density values between each metal and each of the surrounding atoms N_1, N_2, L_1 and L_2 for the most stable sites, together with the values of the Laplacian at these same points. The values of the electron density ρ at the bond critical points connecting the metals with N_1

and N_2 are almost always greater than those connecting them with L_1 and L_2. The only two exceptions are found in site **10** with Zn^{2+} (0.076 au for N_2 and 0.078 au, only 0.002 au above, for L_1, which in this case is Hie) and in site **14** with Al^{3+} (where both N_2 and L_1 have 0.88 au). This indicates a greater strength of the metal-N_1 and metal-N_2 bonds in comparison with the the metal-L_1 and metal-L_2 ones, in agreement with their shorter lengths.

Comparing the values of ρ for Cu^{2+} and Zn^{2+} complexes, one notices that the Cu^{2+} values are always greater than the corresponding Zn^{2+} ones at each site. This fact is indicative of a stronger interaction of the dipeptides with Cu^{2+} rather than with Zn^{2+} (already suggested by distancies and energies). Al^{3+} densities are also higher than Zn^{2+} ones in practically all cases (except for histidines, for which these densities are more similar; compare, for example, the 0.078 au between Zn^{2+} and Hid, which is L_2, at site **4** with the 0.075 au between Al^{3+} and Hid at this same site), so Zn^{2+} is the cation interacting most weakly with the dipeptides. From the comparison of the densities for Cu^{2+} and Al^{3+} one infers that Cu^{2+}-N_1 and Cu^{2+}-N_2 interactions are stronger than Al^{3+}-N_1 and Al^{3+}-N_2 interactions, respectively, and that Asp and Asn interact more favorably with Al^{3+} than with Cu^{2+} (compare, for example, the 0.074 au between Cu^{2+} and Asp, which is L_1, at site **2** with the 0.084 au between Al^{3+} at the same site, and the 0.070 au between Cu^{2+} and Asn, which is again L_1, at site **16** with the 0.082 au between Al^{3+} and Asn at the same site), but Hid and Hie interact better with Cu^{2+} (compare, for example, the 0.081 au between Cu^{2+} and Hid, which is L_2, at site **4** with the 0.075 au between Al^{3+} at the same site).

(a) **(b)**

(c) **(d)**

(e) **(f)**
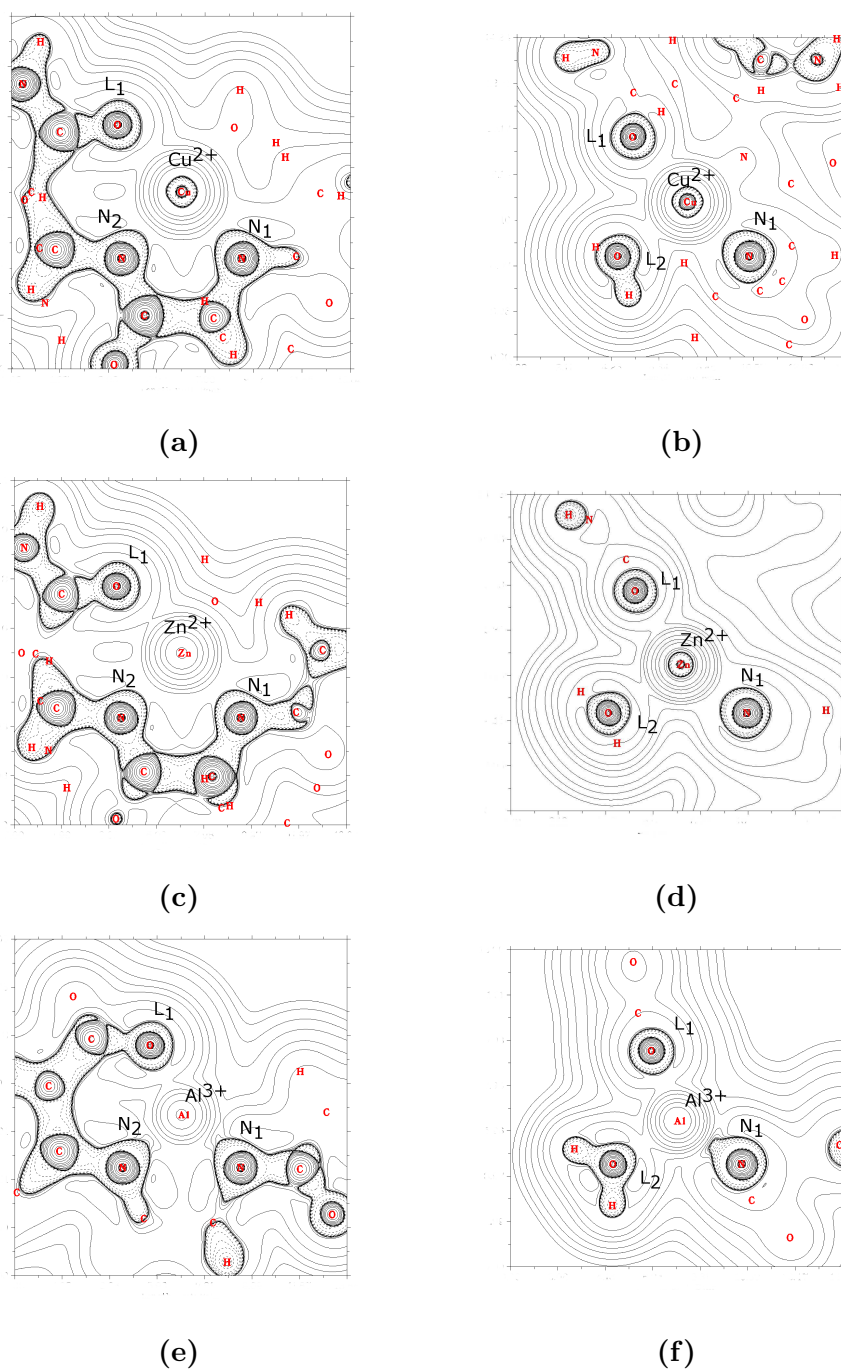
Figure 3.11: Contour plots of the Laplacian of the electron density ($\nabla^2\rho$) for site **16** with Cu^{2+} (*a* and *b*), Zn^{2+} (*c* and *d*) and Al^{3+} (*e* and *f*). The regions of negative $\nabla^2\rho$ are delimited by a thick line. The difference between *a*, *c* and *e*, and *b*, *d* and *f* is that *a*, *c* and *e* are on the N$_1$-N$_2$-L$_1$ plane, while *b*, *d* and *f* are on the N$_1$-L$_2$-L$_1$ plane.

Table 3.7: Electron density (ρ) and its Laplacian ($\nabla^2\rho$) at the bond critical points located on the straight lines that go through Cu^{2+}, Zn^{2+} or Al^{3+} and N_1, N_2, L_1 and L_2 in the most stable sites (**2**, **4**, **6**, **10**, **14**, **15** and **16**). These results were obtained with the M06 functional. Values in au (e^-/Böhr^3 for ρ and e^-/Böhr^5 for $\nabla^2\rho$).

No.	Name	Cu^{2+} $\rho/\nabla^2\rho$	Zn^{2+} $\rho/\nabla^2\rho$	Al^{3+} $\rho/\nabla^2\rho$
2	**1-2-NacMet.Asp.H$_2$O**	N_1 0.093/0.373 N_2 0.101/0.410 L_1 0.074/0.408 L_2 0.057/0.294	N_1 0.088/0.343 N_2 0.085/0.336 L_1 0.068/0.332 L_2 0.051/0.226	N_1 0.088/0.533 N_2 0.089/0.552 L_1 0.086/0.676 L_2 0.068/0.532
4	**1-2-50.NacMet.Asp.Hid**	N_1 0.091/0.359 N_2 0.097/0.391 L_1 0.073/0.396 L_2 0.081/0.350	N_1 0.080/0.304 N_2 0.085/0.338 L_1 0.060/0.277 L_2 0.078/0.311	N_1 0.086/0.518 N_2 0.088/0.542 L_1 0.083/0.647 L_2 0.075/0.438
6	**1-2-50.NacMet.Asp.Hie**	N_1 0.090/0.353 N_2 0.097/0.391 L_1 0.068/0.357 L_2 0.082/0.354	N_1 0.075/0.273 N_2 0.079/0.291 L_1 0.049/0.197 L_2 0.072/0.268	N_1 0.086/0.531 N_2 0.088/0.539 L_1 0.081/0.634 L_2 0.076/0.450
10	**49-50.Val.Hie.H$_2$O**	N_1 0.100/0.398 N_2 0.091/0.352 L_1 0.088/0.384 L_2 0.048/0.222	N_1 0.089/0.331 N_2 0.076/0.276 L_1 0.078/0.302 L_2 0.036/0.128	N_1 0.090/0.549 N_2 0.089/0.543 L_1 0.077/0.454 L_2 0.070/0.548
14	**114-115.Glu.Asp.H$_2$O**	N_1 0.094/0.372 N_2 0.099/0.397 L_1 0.075/0.417 L_2 0.058/0.304	N_1 0.083/0.312 N_2 0.080/0.304 L_1 0.061/0.278 L_2 0.046/0.188	N_1 0.089/0.536 N_2 0.088/0.540 L_1 0.088/0.705 L_2 0.066/0.516
15	**118-119.Val.Asp.H$_2$O**	N_1 0.098/0.393 N_2 0.100/0.399 L_1 0.078/0.443 L_2 0.054/0.272	N_1 0.083/0.311 N_2 0.080/0.302 L_1 0.062/0.286 L_2 0.046/0.187	N_1 0.090/0.542 N_2 0.088/0.541 L_1 0.087/0.694 L_2 0.067/0.520
16	**121-122.Asp.Asn.H$_2$O**	N_1 0.100/0.396 N_2 0.099/0.401 L_1 0.070/0.393 L_2 0.058/0.302	N_1 0.087/0.335 N_2 0.083/0.323 L_1 0.056/0.255 L_2 0.055/0.250	N_1 0.091/0.549 N_2 0.088/0.541 L_1 0.082/0.631 L_2 0.069/0.539

3.4 NBO analysis

Below, the general diagram showing the structure of the complexes studied is reproduced again, in order to remind the nomenclature used.
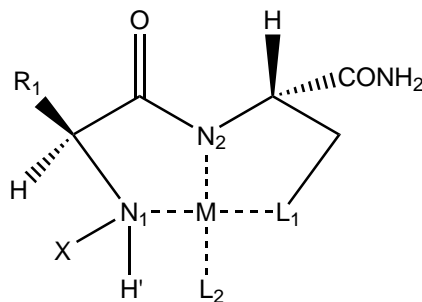

Table 3.8 reports the composition of the NBOs found in the most stable sites (**2**, **4**, **6**, **10**, **14**, **15** and **16**) between the cations Cu^{2+}, Zn^{2+} and Al^{3+} and N_1, N_2, L_1 or L_2, expressed as the percentage of the natural hybrid orbital coming from each atom. These data confirm the high non-covalent character of those bonds (already suggested by the Laplacian of the electron density), since the participation of a hybrid from the cation is never larger than 20.1 % (the Cu^{2+}-N_2 NBO at site **15**, plotted in figure 3.12). It is remarkable that no NBOs involving the cation and one of the four coordinating atoms are found in Zn^{2+} complexes (with the only two exceptions of Zn^{2+}-N_1 in sites **2** and **4**, both with a 8.3 % contribution from Zn^{2+}), suggesting that Zn^{2+} interactions are almost purely non-covalent. In contrast, in Cu^{2+} and Al^{3+} complexes there is a certain degree of covalency (slightly higher for Cu^{2+} than for Al^{3+}).

The Lewis structures for the complexes found by the NBO analysis show a considerable amount of electron delocalization; the percentage of electron population in antibonding (non-Lewis) NBOs is about 2.0 % in all complexes. To this respect, the perturbative analysis of the Fock matrix in the NBO basis indicates that some of the most stabilizing interactions between Lewis-type NBOs and non-Lewis-type NBOs involve the cations and the coordinating atoms N_1, N_2, L_1 and L_2. For example, in the Cu^{2+} complex at site **2**,

Table 3.8: Composition of two-center natural bonding orbitals (NBO) found in each one of the most stable sites (**2**, **4**, **6**, **10**, **14**, **15** and **16**) between each cation and N_1, N_2, L_1 or L_2 (the contribution of the cation is on the left, separated from the contribution of N_1, N_2, L_1 or L_2 by a slash). The lines mean that no NBO was found. Y stands for N_1, N_2, L_1 or L_2. These results were obtained with the M06 functional.

No.	Name	Cu^{2+} % Cu^{2+}/% Y	Zn^{2+} % Zn^{2+}/% Y	Al^{3+} % Al^{3+}/% Y
2	**1-2-NacMet.Asp.H_2O**	N_1 10.7/89.3 N_2 14.8/85.2 L_1 ——— L_2 ———	N_1 8.3/91.7 N_2 ——— L_1 ——— L_2 ———	N_1 10.5/89.5 N_2 9.4/90.6 L_1 2.9/97.1 L_2 ———
4	**1-2-50.NacMet.Asp.Hid**	N_1 ——— N_2 18.9/81.1 L_1 11.2/88.8 L_2 ———	N_1 8.3/91.7 N_2 ——— L_1 ——— L_2 ———	N_1 9.7/90.3 N_2 8.7/91.3 L_1 2.1/97.9 L_2 9.1/90.9
6	**1-2-50.NacMet.Asp.Hie**	N_1 ——— N_2 17.9/82.1 L_1 10.3/89.7 L_2 ———	N_1 ——— N_2 ——— L_1 ——— L_2 ———	N_1 9.2/90.8 N_2 8.6/91.4 L_1 1.7/98.3 L_2 7.3/92.7
10	**49-50.Val.Hie.H_2O**	N_1 15.1/84.9 N_2 18.9/81.1 L_1 10.9/89.1 L_2 ———	N_1 ——— N_2 ——— L_1 ——— L_2 ———	N_1 10.6/89.4 N_2 9.7/90.3 L_1 9.6/90.4 L_2 ———
14	**114-115.Glu.Asp.H_2O**	N_1 15.2/84.8 N_2 19.3/80.7 L_1 9.3/90.7 L_2 ———	N_1 ——— N_2 ——— L_1 ——— L_2 ———	N_1 10.5/89.5 N_2 9.3/90.7 L_1 2.4/97.6 L_2 ———
15	**118-119.Val.Asp.H_2O**	N_1 ——— N_2 20.1/79.9 L_1 11.3/88.7 L_2 ———	N_1 ——— N_2 ——— L_1 ——— L_2 ———	N_1 10.3/89.7 N_2 9.3/90.7 L_1 2.2/97.8 L_2 ———
16	**121-122.Asp.Asn.H_2O**	N_1 16.2/83.8 N_2 18.8/81.2 L_1 8.0/92.0 L_2 ———	N_1 ——— N_2 ——— L_1 ——— L_2 ———	N_1 10.7/89.3 N_2 9.6/90.4 L_1 ——— L_2 ———

the delocalization of the bonding lone pair of N_2 (an $sp^{2.47}$ natural hybrid orbital) into an almost pure antibonding s of Cu^{2+} stabilizes the system by 30.3 kcal/mol, and the delocalization of the bonding lone pair of N_1 (an $sp^{2.29}$
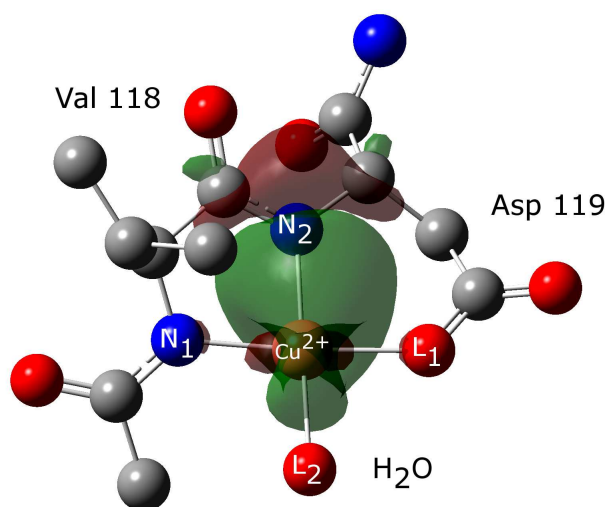
Figure 3.12: Two-center natural bonding orbital connecting Cu^{2+} with N_2 in complex **15**. This is the NBO with the highest contribution from the cation (20.1 %) among all the NBOs found.

natural hybrid) into that same antibonding lone pair of Cu^{2+}, does it by 26.9 kcal/mol. In the Zn^{2+} complex at this same site (**2**), the most stabilizing electron delocalization is from the lone pair of L_1 (the carboxylate oxygen, an $sp^{2.91}$ natural hybrid) into an antibonding lone pair of Zn^{2+} (an $sp^{1.89}d^{0.04}$ natural hybrid), which provides an stabilization of 19.3 kcal/mol. The second most stabilizing donor-acceptor interaction at this site involves the lone pair of N_2 (an $sp^{2.62}$ natural hybrid) and the same antibonding lone pair of Zn^{2+}, with an stabilization of 18.6 kcal/mol. Finally, in the Al^{3+} complex at this same site (**2**), the two most stabilizing interactions of this kind are between the lone pair of the water oxygen (L_2, an $sp^{1.69}$ natural hybrid) and an antibonding lone pair of Al^{3+} (an $sp^{3.67}d^{0.02}$ natural hybrid), with 43.3 kcal/mol, and the delocalization of the lone pair on the carboxylate oxygen (L_1, an $sp^{1.62}$ natural hybrid) into the same antibonding lone pair of Al^{3+}, with an stabilization of 29.5 kcal/mol. Figure 3.13 graphically represents these six interactions.

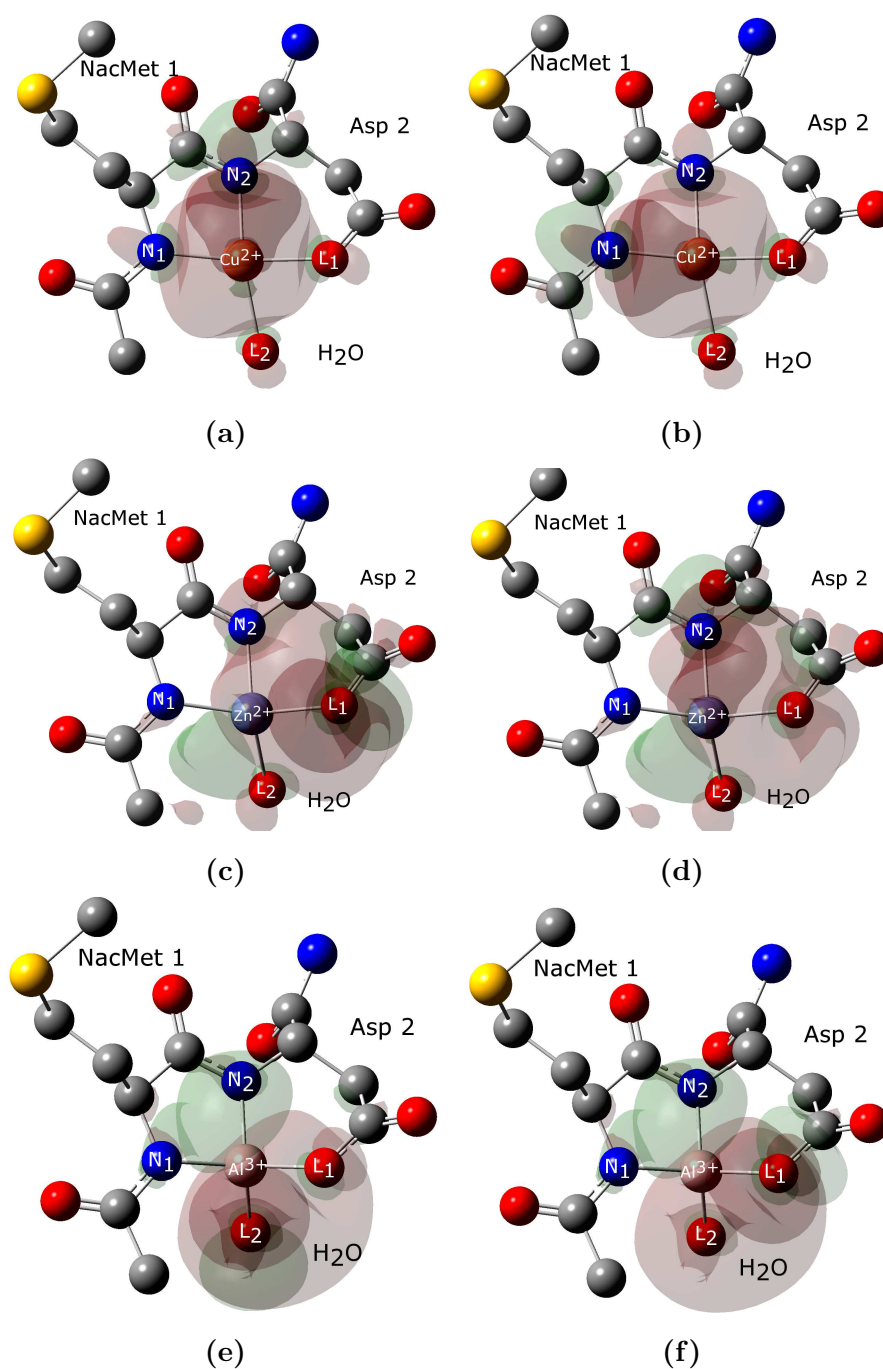**Figure 3.13:** Some of the most stabilizing donor-acceptor interactions (in site **2**) between Cu^{2+}, Zn^{2+} or Al^{3+} and one of the four coordinating atoms. (a): Cu^{2+}-N_2 (30.3 kcal/mol). (b): Cu^{2+}-N_1 (26.9 kcal/mol). (c): Zn^{2+}-L_1 (19.3 kcal/mol). (d): Zn^{2+}-N_2 (18.6 kcal/mol). (e): Al^{3+}-L_2 (43.3 kcal/mol). (f): Al^{3+}-L_1 (29.5 kcal/mol).

Chapter 4

Conclusions

The two main conclusions obtained are the following ones:

- The structural and thermodynamical data about α-synuclein's Cu^{2+} binding sites obtained with the methodology and models used in this work reasonably agree with experiment: Cu^{2+} binds preferentially to Met 1-Asp 2, Val 49-Hie 50 and Asp 121-Asn 122, and its complexes are square planar.

- As a consequence of the previous point, this methodology and these models can be used to study the ability of Cu^{2+} to bind to other, non-explored sites and to make predictions about geometries and energies of complexes with other metals. In relation to this, Cu^{2+} (as well as Zn^{2+} and Al^{3+}) may also bind Glu 114-Asp 115 and Val 118-Asp 119. Also, Al^{3+} (unlike Cu^{2+} and Zn^{2+}) does neither show a particular affinity for Hie 50 nor for Asn 122.

Additional, more specific conclusions are:

- Cu^{2+} complexes are thermodinamically more stable than Zn^{2+} or Al^{3+} ones at the same site, a fact that agrees with experimental findings showing that Cu^{2+} has comparatively higher binding constants.

- The three studied cations show a preference for Asp and Hie (rather than Ser or Thr) as the anchoring site, revealing the role played by electrostatic interactions. This preference is remarkably higher in the case of Al^{3+}.

- Cu^{2+} complexes are always tetracoordinated (with a distorted square planar structure, in agreement with experimental findings), while Zn^{2+} can be both tetracoordinated (with either a distorted square planar or a distorted tetrahedral structure) and tricoordinated, and Al^{3+} complexes are tetracoordinated with a tetrahedral shape.

- The interactions between the three cations studied and the dipeptides are non-covalent (electrostatic), with a slightly higher covalent character in Cu^{2+}.

- All complexes are stabilized by donor-acceptor interactions between the electronegative atoms in the dipeptides or water molecules and empty orbitals on the central cations.

- No meaningful differences arise due to the use of ωB97X-D instead of M06 in geometries. In energies, they generally decrease by an slightly greater amount in the case of Zn^{2+} and Al^{3+} than in the case of Cu^{2+}.

Bibliography

[1] De Lau, L. M. L.; Breteler, M. M. B. (2006) *Epidemiology of Parkinson's disease* Lancet Neurol 5(6): 525-535.

[2] Nuytemans, K.; Theuns, J; Cruts, M; Van Broeckhoven, C. (2010) *Genetic etiology of Parkinson disease associated with mutations in the SNCA, PARK2, PINK1, PARK7, and LRRK2 genes: a mutation update* Hum Mutat 31(7): 763-780.

[3] Lawrence I. Golbe, Margery H. Mark, Jacob I. Sage *Parkinson's Disease Handbook* (New Brunswick, New Jersey, 2010), pp. 1, 23-24.

[4] J. Parkinson *An Essay on the Shaking Palsy* (Whitingham and Rowland, London 1817); W. R. Gowers *A Manual of Diseases of the Nervous System* (Blakiston, Philadelphia, PA, ed. 2, 1893), pp. 6366-6657.

[5] Heisters D (2011) *Parkinson's: symptoms, treatments and research.* Br J Nurs 20(9): 548-554.

[6] William J. Weimer, Lisa M. Schulman, Anthony E. Lang *Parkinson's Disease: A Complete Guide for Patients and Families* (Baltimore, Maryland, ed. 3, 2013), pp. 153-157.

[7] Gibb, W. R. G.; Lees, A. J. (1988) *The relevance of the Lewy body to the pathogenesis of the idiopathic Parkinson's disease* J Neurol Neurosurg Psychiatry 51(6): 745-752.

[8] Esculier, J. F.; Vaudrin, J.; Beriault, P.; Gagnon, K.; Tremblay L. E. (2012) *Home-based balance training programme using Wii Fit with balance board for Parkinson's disease: a pilot study.* J Rehabil Med 44(2): 144-150.

[9] Mhatre Priya, V.; Vilares, I.; Stibb Stacy, M.; Albert Mark, V.; Pickering, L.; Marciniak, C. M.; Kording, K; Toledo, S. (2013) *Wii Fit balance board playing improves balance and gait in Parkinson disease.* PM R 5(9): 769-777.

[10] Goncalves, G. B.; Pereira, J. S.; Leite, M. A. A.; Orsini, M. (2014) *Effects of using the Nintendo Wii Fit Plus platform in the sensorimotor training of gait disorders in Parkinson's disease* Neurol Int 6(1): 5048-5050.

[11] Synnott, J.; Chen, L.; Nugent, C. D.; Moore, G. (2012) *WiiPD–objective home assessment of Parkinson's disease using the Nintendo Wii remote.* IEEE Trans Inf Technol Biomed 16(6): 1304-1312.

[12] Holmes, J. D.; Jenkins, M. E.; Johnson, A. M.; Hunt, M. A.; Clark, R. A. (2013) *Validity of the Nintendo Wii® balance board for the assessment of standing balance in Parkinson's disease.* Clin Rehabil 27(4): 361-366.

[13] Sotirios Parashos, Rosemary L. Wichmann, Todd Melby *Navigating Life with Parkinson Disease* (New York, 2013), pp. 97-105.

[14] Joseph Jankovic, Eduardo Tolosa *Parkinson's Disease and Movement Disorders* (Philadelphia, PA, ed. 5, 2007), pp. 117-118.

[15] Medifocus.com, Inc *Medifocus Guidebook on Parkinson's Disease* (Silver Spring, Maryland, 2011), p. 39.

[16] Mark J. Edwards, Maria Stamelou, Niall Quinn, Kailash P. Bhatia *Parkinson's Disease and other Movement Disorders* (Gosport, Hampshire, ed. 2, 2016), p. 83.

[17] Van Camp, G.; Flamez, A.; Cosyns, B.; Goldstein, J.; Perdaens, C.; Schoors, D. (2003) *Heart valvular disease in patients with Parkinson's disease treated with high-dose pergolide* Neurology 61(6): 859-861.

[18] Robakis, D.; Fahn, S. (2015) *Defining the Role of the Monoamine Oxidase-B Inhibitors for Parkinson's Disease* CNS Drugs 29(6): 433-441.

[19] Finlay, C.; Duty, S. (2014) *Therapeutic potential of targeting glutamate receptors in Parkinson's disease* J Neural Trasm 121(8): 861-880.

[20] Donald G. Grosset, Katherine A. Grosset, Michael S. Okun, Hubert H. Fernandez. *Parkinson's Disease: Clinican's Desk Reference* (Boca Raton, Florida, 2009), p. 115.

[21] Iacono, R. P.; Lonser, R. R.; Morenski, J. D. (1994) *Movement disorders stereotactic surgery for Parkinson's disease* Mov Disord 9(4): 470-472.

[22] Fazzini, E.; Dogali, M.; Sterio, D.; Eidelberg, D.; Beric, A. (1997) *Stereotactic pallidotomy in Parkinson's disease: a long-term follow-up of unilateral pallidotomy* Neurology 48(5):1273-1277.

[23] Chan, D. T.; Mok, V. C.; Poon, W. S.; Hung, K. N.; Zhu, X. L. (2001) *Surgical management of Parkinson's disease: a critical review* Hong Kong Med J 7(1): 34-39.

[24] Gillingham, J. (2000) *Forty-five years of stereotactic surgery for Parkinson's disease: a review* Stereotact Funct Neurosurg 74(3-4): 95-98.

[25] Zimnik, A. J.; Nora, G. J.; Desmurget, M.; Turner, R. S. (2015) *Movement-related discharge in the macaque globus pallidus during high-frequency stimulation of the subthalamic nucleus* J Neurosci 35(9): 3978-3989.

[26] Jafari, N.; Pahwa, R.; Nazzaro, J. M.; Arnold, P. M.; Lyons, K. E. (2016) *MDS-UPDRS to assess non-motor symptoms after STN DBS for Parkinson's disease* Int J Neurosci 126(1): 25-29.

[27] Gardner, J. (2013) *A history of deep brain stimulation: Technological innovation and the role of clinical assessment tools* Soc Stud Sci 43(5): 707-728.

[28] Langston, J. W.; Ballard, P.; Tetrud, J. W.; Irwin, I. (1983) *Chronic Parkinsonism in humans due to a product of meperidine-analog synthesis* Science 219(4587): 979-980.

[29] Javitch, J. A.; D'Amato, R. J.; Strittmatter, S. M.; Snyder, S.H. (1985) *Parkinsonism-inducing neurotoxin, N-methyl-1,4-phenyl-1,2,3,6-tetrahydropyridine: uptake of the metabolite N-methyl-4-phenylpyridinium by dopamine neurons explains selective toxicity* Proc Natl Acad Sci USA 82(7): 2173-2177.

[30] Klaidman, L. K.; Adams, J. D. Jr.; Leung, A. C.; Kim, S. S.; Cadenas, E. (1993) *Redox cycling of MPP$^+$: Evidence for a new mechanism involving hydride transfer with xanthine oxidase, aldehyde dehydrogenase, and lipoamide dehydrogenase* Free Radic Biol Med 15(2): 169-179.

[31] Donovan, D. M.; Miner, L. L.; Perry, M. P.; Revay, R.; Sharpe, L. G.; Przedborski, S.; Kostic, V.; Philbot, R. M.; Kirstein, C. L.; Rothman, R. B.; Schindler, C. W.; Uhl, G. R. (1999) *Cocaine reward and MPTP toxicity: alteration by regional variant dopamine transporter overexpression* Mol Brain Res 73(1,2): 37-49.

[32] Przedborski, S.; Jackson-Lewis, V.; Djaldetti, R.; Liberatore, G.; Vila, M.; Vukosavic, S.; Almer, G. (2000) *The parkinsonian toxin MPTP: action and mechanism* Restor Neurol Neurosci 16(2): 135-142.

[33] Brown, T. P.; Rumsby, P. C.; Capleton, A. C.; Rushton, L.; Levy, L. S. (2006) *Pesticides and Parkinson's disease - is there a link?* Environ Health Perspect 114(2): 156-164.

[34] Payami, H.; Larsen, K.; Bernard, S.; Nutt, J. (1994) *Increased risk of Parkinson's disease in parents and siblings of patients* Ann Neurol 36(4): 659-661.

[35] Marder, K.; Tang, M. X.; Mejia, H.; Alfaro, B.; Cote, L.; Louis, E. (1996) *Risk of Parkinson's disease among first-degree relatives: a community-based study* Neurology 47(1): 155-160.

[36] Kuopio, A.; Marttila, R. J.; Helenius, H.; Rinne, U. K. (2001) *Familial occurrence of Parkinson's disease in a community-based case-control study* Parkinsonism Relat Disord 7(4): 297-303.

[37] Semchuk, K. M.; Love, E. J.; Lee, R. G. (1993) *Parkinson's disease: A test of the multifactorial etiologic hypothesis* Neurology 43(6): 1173-1180.

[38] Ward, C. D.; Duvoisin, R. C.; Ince, S. E.; Nutt, J. D.; Eldridge, R.; Calne, D. B. (1983) *Parkinson's disease in 65 pairs of twins and in a set of quadruplets* Neurology 33(7): 815-824.

[39] Mardsen, C. D. (1986) *Parkinson's disease in twins* J Neurol Neurosurg Psychiatry 50(1): 105-106.

[40] Marttila, R. J.; Kaprio, J.; Koskenvuo, M.; Rinne, U. K. (1988) *Parkinson's disease in a nationwide twin cohort* Neurology 38(8): 1217-1219.

[41] Tanner, C. M.; Ottman, R.; Goldman, S. M.; Ellenberg, J.; Chan, P.; Mayeux, R.; Langston, J. W. (1999) *Parkinson's disease in twins: an etiologic study* JAMA 281(4): 341-346.

[42] Polymeropoulos, M. H.; Higgins, J. J.; Golbe, I. L.; Johnson, W. G.; Ide, S. E.; Di Iorio, G.; Sanges, G.; Stenroos, E. S.; Pho, L. T.; Schaffer, A. A.; Lazzarini, A. M.; Nussbaum, R. L.; Duvoisin, R. C. (1996) *Mapping of a gene for Parkinson's disease to chromosome 4q21-q23* Science 274(5290): 1197-1199.

[43] Polymeropoulos, M. H.; Lavedan, C.; Leroy, E.; Ide, E. S.; Dehejia, A.; Dutra, A.; Pike, B.; Root, H.; Rubenstein, J.; Boyer, R.; Stenroos, E. S.; Chandrasekharappa, S.; Athanassiadou, A.; Papapetropoulos, T.; Johnson, W. G.; Lazzarini, A. M.; Duvoisin, R. C.; Di Iorio, G.; Golbe,

L. I.; Nussbaum, R. L. (1997) *Mutation in the a-synuclein gene identified in families with Parkinson's disease* Science 276(5321): 2045-2047.

[44] Spillantini, M. G.; Schmidt, M. L.; Lee, V. M.; Trojanowski, J. Q.; Jakes, R.; Goedert, M. (1997) *Alpha-synuclein in Lewy bodies* Nature 388(8645): 839-840.

[45] Maroteaux, L.; Campanelli, J. T.; Scheller, R. H. (1988) *Synuclein: a neuron-specific protein localized to the nucleus and presynaptic nerve terminal* J Neurosci 8(8): 2804-2815.

[46] Uéda, K.; Fukushima, H.; Masliah, E.; Xia, Y.; Iwai, A.; Yoshimoto, M.; Otero, D. A. C.; Kondo, J.; Ihara, Y.; Saitoh, T. (1993) *Molecular cloning of cDNA encoding an unrecognized component of amyloid in Alzheimer disease* Proc Natl Acad Sci USA 90(23): 11282-11286.

[47] Weinreb, P. H.; Zhen, W.; Poon, A. W.; Conway, K. A.; Lansbury Jr., P. T. (1996) *NACP, a protein implicated in Alzheimer's disease and learning, is natively unfolded* Biochemistry 35(43): 13709-13715.

[48] Michel, J.; Shen, Y. K.; Aiden, A. P.; Veres, A.; Gray, M. K.; Brockman, W.; The Google Books Team, Pickett, J. P.; Hoiberg, D.; Clancy, D.; Norvig, P.; Orwant, J.; Pinker, S.; Nowak, M. A.; Aiden, E. L. (2011) *Quantitative analysis of culture using millions of digitized books* Science 331(6014): 176-182.

[49] Krüger, R.; Kuhn, W.; Müller, T.; Woitalla, D.; Graeber, M.; Kösel, S.; Przuntek, H.; Epplen, J. T.; Schöls, L.; Riess, O. (1998) *Ala30Pro mutation in the gene encoding a-synuclein in Parkinson's disease* Nat Genet 18(2): 106-108.

[50] Zarranz, J. J.; Alegre, J.; Gómez-Esteban, J. C.; Lezcano, E.; Ros, R.; Ampuero, I.; Vidal, L.; Hoenicka, J.; Rodríguez, O.; Atarés, B.; Llorens, V.; Gómez Tortosa, E.; del Ser, T.; Muñoz, D. G.; de Yebenes, J. G. (2004) *The new mutation, E46K, of a-synuclein, causes Parkinson and Lewy body dementia* Ann Neurol 55(2): 164-173.

[51] Lesage, S.; Anheim, M.; Letournel, F.; Bousset, L.; Honoré, A.; Rozas, N.; Pieri, L.; Madiona, K.; Dürr, A.; Melki, R.; Verny, C.; Brice, A. (2013) *G51D α-synuclein mutation causes a novel Parkinsonian-pyramidal syndrome* Ann Neurol 73(4): 459-471.

[52] Appel-Cresswell, S.; Vilarino-Guell, C.; Encarnacion, M.; Sherman, H.; Yu, I.; Shah, B.; Weir, D.; Thompson, C.; Szu-Tu, C.; Trinh, J.; Aasly, J. O.; Rajput, A.; Rajput, A. H.; Stoessi, A. J.; Farrer, M. J. (2013) *Alpha-synuclein p.H50Q, a novel pathogenic mutation for Parkinson's disease* Movement Disord 28(6): 811-813.

[53] Proukakis, C.; Dudzik, C.; Brier, T.; MacKay, D. S.; Cooper, J. M.; Millhauser, G. L.; Houlden, H.; Schapira, A. H. (2013) *A novel α-synuclein missense mutation in Parkinson disease* Neurology 80(11): 1062-1064.

[54] Pasanen, P.; Myllykangas, L.; Siitonen, M.; Raunio, A.; Kaakkola, S.; Lyytinen, J.; Tienari, P.; Pöyhönen, M.; Paetau, A. (2014) *A novel α-synuclein mutation A53-E associated with atypical multiple system atrophy and Parkinson's disease-type pathology* Ann Neurobiol Aging 35(9): 2180e1-2180e5.

[55] Singleton, A. B.; Farrer, M.; Johnson, J.; Singleton, A.; Hague, S.; Kachergus, J.; Hulihan, M.; Peuralinna, T.; Dutra, A.; Nussbaum, R.; Lincoln, S.; Crawley, A.; Hanson, M.; Maraganore, D.; Adler, C.; Cookson, M. R.; Muenter, M.; Baptista, M.; Miller, D.; Blancato, J.; Hardy, J.; Gwinn-Hardy, K. (2003) *α-synuclein locus triplication causes Parkinson's disease* Science 302(5646): 841.

[56] Chartier-Harlin, M. C.; Kachergus, J.; Roumier, C.; Mouroux, V.; Douay, X.; Lincoln, S.; Levecque, C.; Larvor, L.; Andrieux, J.; Hulihan, M.; Waucquier, N.; Defebvre, L.; Amouyel, P.; Farrer, M.; Destée, A. (2004) *α-synuclein locus duplication as a cause of familial Parkinson's disease* Lancet 364(9440): 1167-1169.

[57] Ibáñez, P.; Bonnet, A. M.; Débarges, B.; Lohmann, E.; Tison, F.; Pol-

lak, P.; Agid, Y.; Dürr, A.; Brice, A. (2004) *Causal relation between α-synuclein gene duplication and familial Parkinson's disease* Lancet 364(9440): 1169-1171.

[58] Cruts, M.; Theuns, J.; Van Broeckhoven, C. (2012) *Locus-specific mutation databases for neurodegenerative brain diseases* Hum Mutat 33(9): 1340-1344.

[59] *Parkinson Disease Mutation Database* `http://www.molgen.vib-ua.be/PDmutDB`

[60] Cheng, F.; Vivacqua, G.; Yu, S. (2011) *The role of alpha-synuclein in neurotransmission and synaptic plasticity* J Chem Neuroanat 42(4): 242-248.

[61] Clayton, D. F.; George, G. M. (1998) *The synucleins: a family of proteins involved in synaptic function, plasticity, neurodegeneration and disease* Trends Neurosci 21(6): 249-254.

[62] Giasson, B. I.; Murray, I. V. J.; Trojanovski, J. Q.; Lee, V. M.-Y. (2001) *A hydrophobic stretch of 12 amino acid residues in the middle of α-synuclein is essential for filament assembly* J Biol Chem 276(4): 2380-2386.

[63] Wu, K.-P.; Weinstock, D. S.; Narayanan, C.; Levy, R. M.; Baum, J. *Structural reorganization of α-synuclein at low pH observed by NMR and REMD simulations* J Mol Biol 391(4): 784-796.

[64] Ulmer, T. S.; Bax, A.; Cole, N. B.; Nussbaum, R. L. (2005) *Structure and dynamics of micelle-bound human alpha-synuclein* J Biol Chem 280(10): 9595-9603.

[65] Uversky, V. N. (2003) *A protein-chameleon: conformational plasticity of α-synuclein, a disordered protein involved in neurodegenerative disorders* J Biomol Struct Dyn 21(2): 211-234.

[66] Berman, H. M.; Westbrook, J.; Feng, Z.; Gilliland, G.; Bhat, T. N.; Weissig, H.; Shindyalov, I. N.; Bourne, P. E. (2000) *The Protein Data Bank* Nucleic Acids Res 28(1): 235-242. `www.rcsb.org`

[67] Schweers, O.; Schönbrunn-Hanebeck, E.; Marx, A.; Mandelkow, E. (1994) *Structural studies of tau protein and Alzheimer paired helical filaments show no evidence for β-structure* J Biol Chem 269(39): 24290-24297.

[68] Kriwacki, R. W.; Hengst, L.; Tennant, L.; Reed, S. I.; Wright, P. E. (1996) *Structural studies of p21$^{Waf1/Cip/Sdi1}$ in the free and Cdk2-bound state: conformational disorder mediates binding diversity* Proc Natl Acad Sci USA 93(21): 11504-11509.

[69] Romero, P.; Obradovic, Z.; Kissinger, C. R.; Villafranca, J. E.; Dunker, A. K. (1997) *Identifying disordered regions in proteins from amino acid sequence* The 1997 IEEE International Conference on Neural Networks Proc 1: 90-95.

[70] Deng, X.; Jesse, E.; Jianlin, C. (2009) *PreDisorder: ab initio sequence-based prediction of protein disordered regions* BMC Bioinformatics 10: 436.

[71] Walsh, I.; Martin, A. J. M.; Di Domenico, T.; Tosatto, S. C. E. (2012) *ESpritz: accurate and fast prediction of protein disorder* Bioinformatics 28(4): 503-509.

[72] Yu, J.; Cao, Z.; Yang, Y.; Wang, C.; Su, Z.; Zhao, Y.; Wang, J.; Zhou, Y. (2016) *Natural protein sequences are more intrinsically disordered than random sequences* Cell Mol Life Sci DOI 10.1007/s00018-016-2138-9.

[73] Bartels, T.; Choi, J. G.; Selkoe, D. J. (2011) *α-synuclein occurs physiologically as a helically folded tetramer that resists aggregation* Nature 477(7362): 107-110.

[74] Wang, W.; Perovic, I.; Chittuluru, J.; Kaganovich, A.; Nguyen, L. T. T.; Liao, J.; Auclair, J. R.; Johnson, D.; Landeru, A.; Simorellis, A. K.; Ju, S.; Cookson, M. R.; Asturias, F. J.; Agar, J. N.; Webb, B. N.; Kang, C.; Ringe, D.; Petsko, G. A.; Pochapsky, T. C.; Hoang, Q. Q. (2011) *A soluble α-synuclein construct forms a dynamic tetramer* Proc Natl Acad Sci 108(43): 17797-17802.

[75] Trexler, A. J.; Rhoades, E. (2012) *N-terminal acetylation is critical for forming α-helical oligomer of α-synuclein* Protein Sci 21(5): 601-605.

[76] Moriarty, G. M.; Janowska, M. K.; Kang, L.; Baum, J. (2013) *Exploring the accessible conformations of N-terminal acetylated α-synuclein* FEBS Lett 587(8): 1128-1138.

[77] Nelson, R.; Eisenberg, D. (2006) *Recent atomic models of amyloid fibril structure* Curr Opin Struc Biol 16(2): 260-265.

[78] Serpell, L. C.; Berriman, J.; Jakes, R.; Goedert, M.; Crowther, R. A. (2000) *Fiber diffraction of synthetic α-synuclein filaments shows amyloid-like cross-β conformation* Proc Natl Acad Sci USA 97(9): 4897-4902.

[79] Vilar, M.; Chou, H.; Lührs, T.; Maji, S. K.; Riek-Loher, D.; Verel, D.; Manning, G.; Stahlberg, H.; Riek, R. (2008) *The fold of α-synuclein fibrils* Proc Natl Acad Sci USA 105(25): 8637-8642.

[80] Procacci, P.; Caminati, G. (2015) *A coarse grain model for α-synuclein aggregation* High Performance Computing on CRESCO infrastructure: research activities and results 2014, December 2015, pp. 98-107.

[81] Ghosh, D.; Singh, P. K.; Sahay, S.; Nath Jha, N.; Jacob, R. S.; Sen, S.; Kumar, A.; Riek, R.; Maji, S. K. (2015) *Structure based aggregation studies reveal the presence of helix-rich intermediate during α-synuclein aggregation* Sci Rep 5: 9228-9242.

[82] Ariesandi, W.; Chang C.; Chen, T.; Chen, Y. (2013) *Temperature-dependent structural changes of Parkinson's alpha-synuclein reveal the role of pre-existing oligomers in alpha-synuclein fibrillization* PLoS One 8(1): e53487.

[83] Bharathi, P.; Nagabhushan, P.; Rao, K. S. J. (2008) *Mathematical approach to understand the kinetics of α-synuclein aggregation: relevance to Parkinson's disease* Comput Biol Med 38(10): 1084-1093.

[84] Yu, H.; Han, W.; Ma, W.; Schulten, K. (2015) *Transient β-hairpin formation in α-synuclein monomer revealed by coarse-grained molecular dynamics simulation* J Chem Phys 143(24): 243142-243156.

[85] Tompkins, M. M.; Hill, W. D. (1997) *Contribution of somal Lewy bodies to neuronal death* Brain Res 775(1-2): 24-29.

[86] Masliah, E.; Rockenstein, E.; Veinbergs, I.; Mallory, M.; Hashimoto, M.; Takeda, A.; Sagara, Y.; Sisk, A.; Mucke, L. (2000) *Dopaminergic loss and inclusion body formation in α-synuclein mice: implications for neurodegenerative disorders* Science 287(5456): 1265-1269.

[87] Volles, M. J.; Lee, S.; Rochet, J.; Shtilerman, M. D.; Ding, T. T.; Kessler, J. C.; Lansbury, P. T. (2001) *Vesicle permeabilization by protofibrillar α-synuclein: implications for the pathogenesis and treatment of Parkinson's disease* Biochemistry 40(26): 7812-7819.

[88] Winner, B.; Jappelli, R.; Maji, S. K.; Desplats, P. A.; Boyer, L.; Aigner, S.; Hetzer, C.; Loher, T.; Vilar, M.; Campioni, S.; Tzitzilonis, C.; Soragni, A.; Jessberger, S.; Mira, H.; Consiglio, A.; Pham, E.; Masliah, E.; Gage, F. H.; Riek, R. (2011) *In vivo demonstration that α-synuclein oligomers are toxic* Proc Natl Acad Sci USA 108(10): 4194-4199.

[89] Apetri, M. M.; Maiti, N. C.; Zagorski, M. G.; Carey, P. R.; Anderson, V. E. (2006) *Secondary structure of α-synuclein oligomers: characterization by Raman and atomic force microscopy* J Mol Biol 355(1): 63-71.

95

[90] Hong, D.; Fink, A. L.; Uversky, V. N. (2008) *Structural characteristics of α-synuclein oligomers stabilized by the flavonoid baicalein* J Mol Biol 383(1): 214-223.

[91] Lashuel, H. A.; Hartley, D.; Petre, B. M.; Walz, T.; Lansbury Jr, P. T. (2002) *Amyloid pores from pathogenic mutations* Nature 418(6895): 291.

[92] Tsigelny, I. F.; Bar-On, P.; Sharikov, Y.; Crews, L.; Hashimoto, M.; Miller, M. A.; Keller, S. H.; Platoshyn, O.; Yuan, J. X.-J.; Masliah, E. (2007) *Dynamics of α-synuclein aggregation and inhibition of pore-like oligomer development by β-synuclein* FEBS J 274(7): 1862-1877.

[93] Volles, M. J.; Lansbury Jr., P. T. (2002) *Vesicle permeabilization by protofibrillar α-synuclein is sensitive to Parkinson's disease-linked mutations and occurs by a pore-like mechanism* Biochemistry 41(14): 4595-4602.

[94] Kayed, R.; Pensalfini, A.; Margol, L.; Sokolov, Y.; Sarsoza, F.; Head, E.; Hall, J.; Glabe, C. (2009) *Annular protofibrils are a structurally and functionally distinct type of amyloid oligomer* J Biol Chem 284(7): 4230-4237.

[95] Jin, J.; Li, G. J.; Davis, J.; Zhu, D.; Wang, Y.; Pan, C.; Zhang, J. (2006) *Identification of novel proteins associated with both α-synuclein and DJ-1* Mol Cell Proteomics 6(5): 845-859.

[96] Hedge, M. L.; Rao, K. S. J. (2003) *Challenges and complexities of α-synuclein toxicity: new postulates in unfolding the mystery associated with Parkinson's disease* Arch Biochem Biophys 418(2): 169-178.

[97] Uversky, V. N.; Li, J.; Souillac, P.; Millett, I. S.; Doniach, S.; Jakes, R.; Goedert, M.; Fink, A. L. (2002) *Biophysical properties of the synucleins and their propensities to fibrillate* J Biol Chem 277(14): 11970-11978.

[98] Shashidharan, P.; Good, P. F.; Hsu, A.; Perl, D. P.; Brin, M. F.; Olanow, C. W. (2000) *TorsinA accumulation in Lewy bodies in sporadic Parkinson's disease* Brain Res 877(2): 379-381.

[99] Lo Bianco, C.; Shorter, J.; Réqulier, E.; Lashuel, H.; Iwatsubo, T.; Lindquist, S.; Aebischer, P. (2008) *Hsp104 antagonizes alpha-synuclein aggregation and reduces dopaminergic degeneration in a rat model of Parkinson's disease* J Clin Invest 118(9): 3087-3097.

[100] Pountney, D. L.; Treweek, T. M.; Chataway, T.; Huang, Y.; Chegini, F.; Blumbergs, P. C.; Raffery, M. J.; Gai, W. P. (2005) *Alpha B-crystallin is a major component of glial cytoplasmic inclusions in multiple system atrophy* Neurotox Res 7(1-2): 77-85.

[101] Zhu, M.; Han, S.; Fink, A. L. (2013) *Oxidized quercetin inhibits α-synuclein fibrillization* Biochim Biophys Acta 1830(4): 2872-2881.

[102] Cheng, X. R.; Kerman, K. (2015) *Electrochemical detection of interaction between α-synuclein and clioquinol* Electroanal 27(6): 1436-1442.

[103] Silva, B. A.; Einarsdóttir, O.; Fink, A. L.; Uversky, V. N. (2013) *Biophysical characterization of α-synuclein and rotenone interaction* Biomolecules 3(3): 703-732.

[104] Gerard, M. Z.; Desender, D. L.; Baert, J.; Baekelandt, B. V.; Engelborghs, Y. (2008) *Fk506 binding protein 12 differentially accelerates fibril formation of wild type alpha-synuclein and its clinical mutants a30p or a53t* J Neurochem 106(1): 121-133.

[105] Jayaraj, R. L.; Ranjani, V.; Manigandan, K.; Elangovan, N. (2013) *Insilico docking studies to identify potent inhibitors of alpha-synuclein aggregation in Parkinson's disease* Asian J Pharm Clin Res 6(Suppl. 4): 127-131.

[106] Beyer, K. (2006) *α-synuclein structure, posttranslational modification and alternative splicing as aggregation enhancers* Acta Neuropathol

112(3): 237-251.

[107] Fujiwara, H.; Hasegawa, M.; Dohmae, N.; Kawashima, A.; Masliah, E.; Goldberg, M. S.; Shen, J.; Takio, K.; Iwatsubo, T. (2002) *a-synuclein is phosphorylated in synucleinopathy lesions* Nat Cell Biol 4(2): 160-164.

[108] Okochi, M.; Walter, J.; Koyama, A.; Nakajo, S.; Baba, M.; Iwatsubo, T.; Meijer, L.; Kahle, P. J.; Haass, C. (2000) *Constitutive phosphorylation of the Parkinson's disease associated a-synuclein* J Biol Chem 275(1): 390-397.

[109] Ellis, C. E.; Schwartzberg, P. L.; Grider, T. L.; Fink, D. W.; Nussbaum, R. L. (2001) *a-synuclein is phosphorylated by members of the Src family of protein-tyrosine kinases* J Biol Chem 276(6): 3879-3884.

[110] Smith, W. W.; Margolis, R. L.; Li, X.; Troncoso, J. C.; Lee, M. K.; Dawson, V. L.; Dawson, T. M.; Iwatsubo, T.; Ross, C. A. (2005) *a-synuclein phosphorylation enhances eosinophilic cytoplasmic inclusion formation in SH-SY5Y cells* J Neurosci 25(23): 5544-5552.

[111] Anderson, J. P.; Walker, D. E.; Goldstein, J. M.; Laat, R.; Banducci, K.; Caccavello, R. J.; Barbour, R.; Huang, J.; Kling, K.; Lee, M.; Diep, L.; Keim, P. S.; Shen, X.; Chataway, T.; Schlossmacher, M. G.; Seubert, P.; Schenk, D.; Sinha, S.; Gai, W. P.; Chilcote, T. J. (2006) *Phosphorylation of Ser-129 is the dominant pathological modification of a-synuclein in familial and sporadic Lewy body disease* J Biol Chem 281(40): 29739-29752.

[112] Chen, L.; Periquet, M.; Wang, X.; Negro, A.; McLean, P. J.; Hyman, B. T.; Feany, M. B. (2009) *Tyrosine and serine phosphorylation of a-synuclein have opposing effects on neurotoxicity and soluble oligomer formation* J Clin Invest 119(11): 3257-3265.

[113] Giasson, B. I.; Duda, J. E.; Murray, I. V. J.; Chen, Q., Souza, J. M.; Hurtig, H. I.; Ischiropoulos, H.; Trojanowski, J. Q.; Lee, V. M.-Y. (2000)

Oxidative damage linked to neurodegeneration by selective a-synuclein nitration in synucleinopathy lesions Science 290(5493): 985-989.

[114] Ischiropoulos, H. (1998) *Biological tyrosine nitration: a pathophysiological function of nitric oxide and reactive oxygen species* Arch Biochem Biophys 356(1): 1-11.

[115] Souza, J. M.; Giasson, B. I.; Chen, Q.; Lee, V. M.-Y.; Ischiropoulos, H. (2000) *Dityrosine cross-linking promotes formation of stable a-synuclein polymers* J Biol Chem 275(24): 18344-18349.

[116] Burai, R.; Ait-Bouziad, N.; Chiki, A.; Lashuel, H. A. (2015) *Elucidating the role of site-specific nitration of a-synuclein in the pathogenesis of Parkinson's disease via protein semisynthesis and mutagenesis* J Am Chem Soc 137(15): 5041-5052.

[117] Hokenson, M. J.; Uversky, V. N.; Goers, J.; Yamin, G.; Munishkina, L. A.; Fink, A. L. (2004) *Role of individual methionines in the fibrillation of methionine-oxidized a-synuclein* Biochemistry 43(15): 4621-4633.

[118] Uversky, V. N.; Yamin, G.; Souillac, P. O.; Goers, J.; Glaser, C. B.; Fink, A. L. (2002) *Methionine oxidation inhibits fibrillaion of human a-nynuclein in vitro* FEBS Let 517(1-3): 239-244.

[119] Carmo-Gonçalves, P.; Pinheiro, A. S.; Romão, L.; Cortines, J.; Follmer, C. (2014) *UV-induced selective oxidation of Met5 to Met-sulfoxide leads to the formation of neurotoxic fibril-incompetent a-synuclein oligomers* Amyloid 21(3): 163-174.

[120] Guerrero, E.; Vasudevaraju, P.; Hegde, M. L.; Britton, G. B.; Rao, K. S. (2013) *Recent advances in a-synuclein functions, advanced glycation, and toxicity: implications for Parkinson's disease* Mol Neurobiol 47(2): 525-536.

[121] Salahuddin, P.; Rabbani, G.; Khan, R. H. (2014) *The role of advanced glycation end products in various types of neurodegenerative disease: a*

therapeutic approach Cell Mol Biol Lett 19(3):407-437.

[122] Miranda, H. V.; Outeiro, T. F. (2010) *The sour side of neurodegenerative disorders: the effects of protein glycation* J Pathol 221(1): 13-25.

[123] Castellani, R.; Smith, M. A.; Richey, P. L.; Perry, G. (1996) *Glycoxidation and oxidative stress in Parkinson disease and diffuse Lewy body disease* Brain Res 737(1-2): 195-200.

[124] Dalfó, E.; Portero-Otín, M.; Ayala, V.; Martínez, A.; Pamplona, R.; Ferrer, I. (2005) *Evidence of oxidative stress in incidental Lewy body disease* J Neuropathol Exp Neurol 64(9): 816-830.

[125] Lee, D.; Park, C. W.; Paik, S. R.; Choi, K. Y. (2009) *The modification of α-synuclein by dicarbonyl compounds inhibits its fibril-forming process* Biochim Biophys Acta 1794(3): 421-430.

[126] Reddy, V. P.; Beyaz, A. (2006) *Inhibitors of the Maillard reaction and AGE breakers as therapeutics for multiple diseases* Drug Discov Today 11(13-14): 646-654.

[127] Soppa, J. (2010) *Protein acetylation in archaea, bacteria and eukaryotes* Archaea 2010, Article ID 820681, 9 pages, doi:10.1155/2010/820681.

[128] Polevoda, B.; Sherman, F. (2003) *N-terminal acetyltransferases and sequence requirements for N-terminal acetylation of eukaryotic proteins* J Mol Biol 325(4): 595-622.

[129] Zabrocki, P.; Bastiaens, I.; Delay, C.; Bammens, T.; Ghillebert, R.; Pellens, K.; De Virgilio, C.; Van Leuven, F.; Winderickx, J. (2008) *Phosphorylation, lipid raft interaction and traffic of alpha-synuclein in a yeast model for Parkinson* Biochim Biophys Acta 1783(10): 1767-1780.

[130] Fauvet, B.; Fares, M-B; Samuel, F.; Dikiy, I.; Tandon, A.; Eliezer, D.; Lashuel, H. A. (2012) *Characterization of semisynthetic and natu-*

rally N^α-acetylated α-synuclein in vitro and in intact cells J Biol Chem 287(34): 28243-28262.

[131] Maltsev, A. S.; Ying, J.; Bax, A. (2012) *Impact of N-terminal acetylation of α-synuclein on its random coil and lipid binding properties* Biochemistry 51(25): 5004-5013.

[132] Kang, L.; Moriarty, G. M.; Woods, L. A.; Ashcroft, A. E.; Radford, S. E.; Baum, J. (2012) *N-terminal acetylation of α-synuclein induces increased transient helical propensity and decreased aggregation rates in the intrinsically disordered monomer* Prot Sci 21(7): 911-917.

[133] Zayed, J.; Ducic, S.; Campanella, G.; Panisset, J. C.; Andre, P.; Masson, H.; Roy, M. (1990) *Environmental factors in the etiology of Parkinson's disease* Can J Neurol Sci 17(3): 286-291.

[134] Rybicki, B. A.; Johson, C. C.; Uman, J.; Gorell, J. M. (1993) *Parkinson's disease mortality and the industrial use of heavy metals in Michigan* Mov Disord 8(1): 87-92.

[135] Gorell, J. M.; Johnson, C. C.; Rybicki, B. A.; Peterson, E. L.; Kortsha, G. X.; Brown, G. G.; Richardson, R. J. (1997) *Occupational exposure to metals as risk factors for Parkinson's disease* Neurology 48(3): 650-658.

[136] Riederer, P.; Sofic, E.; Rausch, W. D.; Schmidt, B. Reynolds, G. P.; Jellinger, K.; Youdim, M. B. (1989) *Transition metals, ferritin, glutathione, and ascorbic acid in parkinsonian brains* J Neurochem 52(2): 515-520.

[137] Dexter, D. T.; Carayon, A.; Javoy-Agid, F.; Agid, Y.; Wells, F. R.; Daniel, S. E.; Lees, A. J.; Jenner, P.; Marsden, C. D. (1991) *Alterations in the levels of iron, ferritin and other trace metals in Parkinson's disease and other neurodegenerative diseases affecting the basal ganglia* Brain 114(4): 1953-1975.

[138] Youdim, M. B.; Ben Shachar, D.; Riederer, P. (1991) *Iron in brain function and dysfunction with emphasis on Parkinson's disease* Eur Neurol 31(Suppl 1): 34-40.

[139] Uversky, V. N.; Li, J.; Fink, A. L. (2001) *Metal-triggered structural transformations, aggregation, and fibrillation of human a-synuclein* J Biol Chem 276(47): 44284-44296.

[140] Davies, P.; Moualla, D.; Brown, D. R. (2011) *Alpha-synuclein is a cellular ferrireductase* PLoS One 6(1): e15814.

[141] Sung, Y.; Rospigliosi, C.; Eliezer, D. (2006) *NMR mapping of copper binding sites in alpha-synuclein* Biochim Biophys Acta 1764(1): 5-12.

[142] Rasia, R. M.; Bertoncini, C. W.; Marsh, D.; Hoyer, W.; Cherny, D.; Zweckstetter, M.; Griesinger, C.; Jovin, T. M.; Fernández, C. O. (2005) *Structural characterization of copper(II) binding to a-synuclein: Insights into the bioinorganic chemistry of Parkinson's disease* Proc Natl Acad Sci USA 102(12): 4294-4299.

[143] Bortolus, M.; Bisaglia, M.; Zoleo, A.; Fittipaldi, M.; Benfatto, M.; Bubacco, L.; Maniero, A. L. (2015) *Structural characterization of a high affinity mononuclear site in the copper(II)-a-synuclein complex* J Am Chem Soc 132(51): 18057-18066.

[144] De Ricco, R.; Valensin, D.; Dell'Acqua, S.; Casella, L.; Dorlet, P.; Faller, P.; Hureau, C. (2015) *Remote His50 acts as a coordination switch in the high-affinity N-terminal centered copper(II) site of a-synuclein* (2015) Inorg Chem 54(10): 4744-4751.

[145] Camponeschi, F.; Valensin, D.; Tessari, I.; Bubacco, L.; Dell'Acqua, S.; Casella, L.; Monzani, E.; Gaggelli, E.; Valensin, G. (2013) *Copper(I)-a-synuclein interaction: structural description of two independent and competing metal binding sites* Inorg Chem 52(3): 1358-1367.

[146] Tabner, B. J.; Turnbull, S.; El-Agnaf, O. M. A.; Allsop, D. (2002) *Formation of hydrogen peroxide and hydroxyl radicals from Aβ and α-synuclein as a possible mechanism of cell death in Alzheimer's disease and Parkinson's disease* Free Radic Biol Med 32(11): 1076-1083.

[147] Binolfi, A.; Rasia, R. M.; Bertoncini, C. W.; Ceolin, M.; Zweckstetter, M.; Griesinger, C.; Jovin, T. M.; Fernández, C. O. (2006) *Interaction of α-synuclein with divalent metal ions reveals key differences: a link between structure, binding specificity and fibrillation enhancement* J Am Chem Soc 128(30): 9893-9901.

[148] Peng, Y.; Wang, C.; Xu, H. H.; Liu, Y-N.; Zhow, F. (2010) *Binding of α-synuclein with Fe(III) and with Fe(II) and biological implications of the resultant complexes* J Inorg Biochem 104(4): 365-370.

[149] Valiente-Gabioud, A. A.; Torres-Monserrat, V.; Molina-Rubino, L.; Binolfi, A.; Griesinger, C.; Fernández, C. O. (2012) *Structural basis behind the interaction of Zn^{2+} with the protein α-synuclein and the Aβ peptide: a comparative analysis* J Inorg Biochem 117: 334-341.

[150] Bader, R. F. W. (2002) *Atoms in Molecules* Encyclopedia of Computational Chemistry.

[151] Reed, A. E.; Curtiss, L. A.; Weinhold, F. (1988) *Intermolecular interactions from a natural bond orbital, donor-acceptor viewpoint* Chem Rev 88: 899-926.

[152] Binolfi, A.; Rodríguez, E. E.; Valensin, D.; D'Amelio, N.; Ippoliti, E.; Obal, G.; Duran, R.; Magistrato, A.; Pritsch, O.; Zweckstetter, M.; Valensin, G.; Carloni, P.; Quintanar, L.; Griesinger, C.; Fernández, C. O. (2010) *Bioinorganic chemistry of Parkinson's disease: structural determinants for the copper-mediated amyloid formation of alpha-synuclein* Inorg Chem 49(22): 10668-10679.

[153] Sóvágó, I.; Kállay, C.; Várnagy, K. (2012) *Peptides as complexing agents: factors influencing the structure and thermodynamic stability*

of peptide complexes Coordin Chem Rev 256(19-20): 2225-2233.

[154] Zhao, Y.; Truhlar, D. G. (2008) *The M06 suite of density functionals for main group thermochemistry, thermochemical kinetics, noncovalent interactions, excited states, and transition elements: two new functionals and systematic testing of four M06-class functionals and 12 other functionals* Theor Chem Account 120(1-3): 215-241.

[155] Marenich, A. V.; Cramer, C. J.; Truhlar, D. G. (2008) *Universal solvation model based on solute electron density and on a continuum model of the solvent defined by the bulk dielectric constant and atomic surface tensions* J Phys Chem B 113(18): 6378-6396.

[156] Chai, J-D.; Head-Gordon, M. (2008) *Long-range corrected hybrid density functionals with damped atom-atom dispersion corrections* Phys Chem Chem Phys 10(44): 6615-6620.

[157] Gaussian 09, Revision B.01, Frisch, M. J.; Trucks, G. W.; Schlegel, H. B.; Scuseria, G. E.; Robb, M. A.; Cheeseman, J. R.; Scalmani, G.; Barone, V.; Mennucci, B.; Petersson, G. A.; Nakatsuji, H.; Caricato, M.; Li, X.; Hratchian, H. P.; Izmaylov, A. F.; Bloino, J.; Zhen, G.; Sonnenberg, J. L.; Hada, M.; Ehara, M.; Toyota, K.; Fukuda, R.; Hasegawa, J.; Ishida, M.; Nakajima, T.; Honda, Y.; Kitao, O.; Nakai, H.; Vreven, T.; Montgomery, Jr., J. A.; Peralta, J. E.; Ogliaro, F.; Bearpark, M.; Heyd, J. J.; Brothers, E.; Kudin, K. N.; Staroverov, V. N.; Keith, T.; Kobayashi, R.; Normand, J.; Raghavachari, K.; Rendell, A.; Burant, J. C.; Iyengar, S. S.; Tomasi, J.; Cossi, M.; Rega, N.; Millam, J. M.; Klene, M.; Knox, J. E.; Cross, J. B.; Bakken, V.; Adamo, C.; Jaramillo, J.; Gomperts, R.; Stratmann, R. E.; Yazyev, O.; Austin, A. J.; Cammi, R.; Pomelli, C.; Ochterski, J. W.; Martin, R. L.; Morokuma, K.; Zakrzewski, V. G.; Voth, G. A.; Salvador, P.; Dannenberg, J. J.; Dapprich, S.; Daniels, A. D.; Farkas, O.; Foresman, J. B.; Ortiz, J. V.; Cioslowski, J. and Fox, D. J., Gaussian, Inc., Wallingford CT, 2010.

[158] NBO Version 3.1. Glendening, E. D.; Reed, A. E.; Carpenter, J. E. and Weinhold, F.

[159] Multiwfn -A Multifunctional Wavefunction Analyzer. `https://multiwfn.codeplex.com`

[160] Shil, S.; Bhattacharya, D.; Sarkar, S.; Misra, A. (2013) *Performance of the widely used Minnesota density functionals for the prediction of heat of formations, ionization potentials of some benchmarked first row transition metal complexes* J Phys Chem A 117(23): 4945-4955.

[161] Wang, Y.; Wu, W.; Liu, Y.; Lu, Y. (2013) *Influence of transition metal coordination on halogen bonding: CSD survey and theoretical study* Chem Phys Lett 578: 38-42.

[162] Nose, H.; Rodgers, M. T. (2014) *Influence of the d orbital occupation on the structures and sequential binding energies of pyridine to the late first-row divalent transition metal cations: a DFT study* J Chem Phys A 118(37): 8129-8140.

[163] Chai, J-D.; Head-Gordon, M. (2008) *Systematic optimization of long-range corrected hybrid density functionals* J Chem Phys 128(8): 084106.

[164] Grimme, S. (2006) *Semiempirical GGA-type density functional constructed with a long-range dispersion correction* J Comput Chem 27(15): 1787-1799.

[165] Tomasi, J.; Mennucci, B.; Cancès, E. (1999) *The IEF version of the PCM solvation method: an overview of a new method addressed to study molecular solutes at the QM ab initio level* J Mol Struct Theochem 464(1-3): 211-226.

[166] Gaussian 09 User's Reference, `http://www.gaussian.com/g_tech/g_ur/k_scrf.htm`

[167] Ochterski, J. W. (2000) *Thermochemistry in Gaussian* `http://www.gaussian.com/g_whitepap/thermo.htm`